

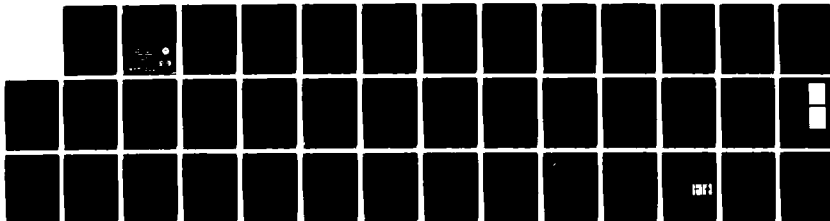
AD-A139 591 INTFL - 8401 COMPUTER TOMOGRAPHY FOR INTERFEROMATIC
AERODYNAMIC MEASUREMENTS(U) MICHIGAN UNIV ANN ARBOR
INTERFEROMETRY LAB C M VEST 1984 ARO-17698.4-EG

1/0

UNCLASSIFIED DAAG29-81-K-0015

F/G 9/2

NL



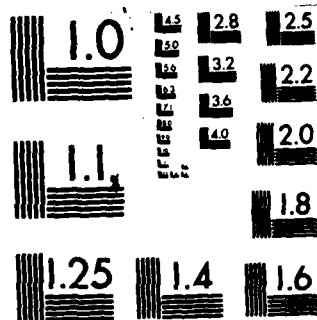
END

DATE

FILED

5-5-84

DTIC



MICROCOPY RESOLUTION TEST CHART
NATIONAL BUREAU OF STANDARDS-1963-A

ARO 17698400

②

AD A139591

INTFL - 8481
COMPUTER TOMOGRAPHY
FOR
INTERFEROMETRIC AERODYNAMIC MEASUREMENTS

Final Report

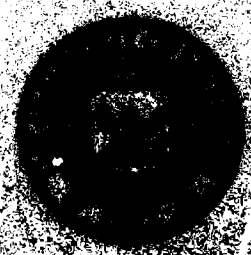
C.M. Vest

Office of Research

Department of

Mechanical Engineering

University of Michigan



Unclassified

SECURITY CLASSIFICATION OF THIS PAGE (When Data Entered)

REPORT DOCUMENTATION PAGE		READ INSTRUCTIONS BEFORE COMPLETING FORM
1. REPORT NUMBER ARO 17698.4-EG	2. GOVT ACCESSION NO. A13939	3. RECIPIENT'S CATALOG NUMBER
4. TITLE (and Subtitle) Interferomatic Aerodynamic Measurements		5. TYPE OF REPORT & PERIOD COVERED Final Report 20 Oct 1980-31 Dec 1983
		6. PERFORMING ORG. REPORT NUMBER
7. AUTHOR(s) C. M. Vest		8. CONTRACT OR GRANT NUMBER(s)
9. PERFORMING ORGANIZATION NAME AND ADDRESS Michigan, Univ		10. PROGRAM ELEMENT, PROJECT, TASK AREA & WORK UNIT NUMBERS N/A
11. CONTROLLING OFFICE NAME AND ADDRESS U. S. Army Research Office Post Office Box 12211 Research Triangle Park, NC 27709		12. REPORT DATE 1984
		13. NUMBER OF PAGES 34
14. MONITORING AGENCY NAME & ADDRESS (if different from Controlling Office)		15. SECURITY CLASS. (of this report) Unclassified
		15a. DECLASSIFICATION/DOWNGRADING SCHEDULE
16. DISTRIBUTION STATEMENT (of this Report) Approved for public release; distribution unlimited.		
17. DISTRIBUTION STATEMENT (of the abstract entered in Block 20, if different from Report)		
18. SUPPLEMENTARY NOTES The view, opinions, and/or findings contained in this report are those of the author(s) and should not be construed as an official Department of the Army position, policy, or decision, unless so designated by other documentation		
19. KEY WORDS (Continue on reverse side if necessary and identify by block number) Holography Computers Tomography Interferometry Aerodynamics		
20. ABSTRACT (Continue on reverse side if necessary and identify by block number) Under this research program we have studied and developed several topics associated with the use of multidirectional holographic interferometry with data analysis by computer tomography for application to complex aerodynamic flows. In this		

ARQ 17698.4-EG

20. ABSTRACT CONTINUED

technique, interferometric data are recorded virtually instantaneously by pulsed laser holographic interferometry and later are read out photometrically, digitized, and then processed by a computer to produce density maps in a set of planar cross sections of a three-dimensional flow. This program has included development of computer tomography codes of a new type, development of a microcomputer-controlled system for scanning interferograms and preprocessing the data, initial development of a new (non-holographic) hybrid optical/digital technique for recording information equivalent to that normally recorded on an interferogram of a flow, the execution of a simple prototype experiment, and considerable progress toward development of instrumentation for three-dimensional density measurement in a low-speed wind tunnel.

Unclassified

SECURITY CLASSIFICATION OF THIS PAGE(When Data Entered)

I N T F L - 8 4 0 1
COMPUTER TOMOGRAPHY
FOR
INTERFEROMATIC AERODYNAMIC MEASUREMENTS

Final Report

C.M. Vest

Accession For	
NTIS GRA&I	<input checked="" type="checkbox"/>
DTIC TAB	<input type="checkbox"/>
Unannounced	<input type="checkbox"/>
Justification	
Distribution/	
Availability Codes	
Avail and/or	
Spec	Special
A-1	

I N T F L - 8 4 0 1

FINAL REPORT

20 October 1980 through 31 December 1983

C.M. Vest

February 1984

Interferometry Laboratory

Department of Mechanical Engineering & Applied Mechanics

The University of Michigan

Ann Arbor, Michigan 48109

Prepared for Army Research Office

Contract Number DAAG29-81-K-0015


TABLE OF CONTENTS

1.	INTRODUCTION.....	1
2.	PROBLEM STATEMENT.....	1
3.	SUMMARY OF IMPORTANT RESULTS.....	3
3.1	Interference Fringe Scanning and Processing.....	3
3.1.1	Scanning System.....	3
3.1.2	Fringe Analysis.....	4
3.2	Tomographic Algorithm Development.....	5
3.2.1	Reconstruction of Strongly Refracting Fields...6	
3.2.2	The Iterative Convolution Method.....	7
3.3	Experimentation.....	9
3.3.1	Demonstration Experiment.....	10
3.3.2	Wind Tunnel Experimentation.....	10
3.4	Hybrid Processor for Wavefront Recording.....	11
4.	PUBLICATIONS.....	13
4.1	Journal Articles.....	13
4.2	Presentations at Technical Meetings.....	13
4.3	Reports.....	14
5.	PARTICIPATING SCIENTIFIC PERSONNEL.....	14
6.	APPENDIX.....	16

1. INTRODUCTION

This is the final report for the project entitled "Computer Tomography for Interferometric Aerodynamic Measurements" sponsored in the Department of Mechanical Engineering and Applied Mechanics at The University of Michigan by the Army Research Office during the period 20 October 1980 through 31 December 1983 under Contract Number DAAG29-81-K-0015.

2. PROBLEM STATEMENT

the author has
Under this research program ~~we have~~ studied and developed several topics associated with the use of multidirectional holographic interferometry with data analysis by computer tomography for application to complex aerodynamic flows. In this technique, interferometric data are recorded virtually instantaneously by pulsed laser holographic interferometry and later are read out photometrically, digitized, and then processed by a computer to produce density maps in a set of planar cross sections of a three-dimensional flow. This program has included development of computer tomography codes of a new type, development of a microcomputer-controlled system for scanning interferograms and preprocessing the data, initial development of a new (non-holographic) hybrid optical/digital technique for recording information equivalent to that normally recorded on an interferogram of a flow, the execution of a simple prototype experiment, and considerable progress toward development of instrumentation for three-dimensional density measurement in a low-speed wind tunnel. 

This program has been developed on the premise that experimental fluid dynamics will be dominated by methods which combine laser diagnostics with computer control and analysis. To date most work in the field has emphasized local, time-resolved techniques such as laser doppler velocimetry and various types of spectroscopy which have high accuracy but do not yield understanding of global features of flows except by collection of vast amounts of data from repeated experiments. The current research project has been devoted to the development of techniques which provide instantaneous, whole-field measurements of aerodynamic density, generally with lower accuracy and spatial resolution than the local techniques. Techniques of these two types are thus complementary, although the whole-field techniques are in great need of basic development. Although we have considered very general aspects of the problem of measurement of three-dimensional density fields, the work we have conducted is believed to have relevance to efforts such as that at the Army Aeromechanics Laboratory to use holographic interferometry to study the aerodynamics of compressible flow near helicopter blades.

Holographic interferometry is the interferometric comparison of two optical waves, at least one of which has been recorded holographically. This technique can be used to produce interferograms which can be viewed from several different directions. These interferograms can be recorded in approximately 20 ns using a pulsed laser, and they can be viewed,

manipulated and analyzed after the flow experiment has been completed. Computer tomography is a technique for computationally reconstructing two- or three-dimensional objects from measured projections, or line integrals through them. In this case, the data are line integrals of fluid refractive index determined by examining the holographic interferogram from several different directions. The result of such a computer tomographic analysis is a map of the density distribution in any cross sectional plane of the flow.

Key topics which we believed at the outset needed research in order to fully develop the potential of these techniques were augmented during the research by other tasks whose importance became apparent during the program. These topics can be categorized as Interference Fringe Scanning and Processing, Tomographic Algorithm Development, Alternate Technique for Wavefront Recording, and Experimentation.

3. SUMMARY OF IMPORTANT RESULTS

In this section we outline the key results obtained during the research program. In most cases, these results have been fully documented in journal articles, which are referenced in the text of this report.

3.1 Interference Fringe Scanning and Processing

3.1.1 Scanning System

We have constructed a system to record the irradiance distribution (fringe pattern) of the waves of laser

light reconstructed using holograms of aerodynamic flows. The system can be used to directly view the reconstructed waves without the need for extra viewing optics. The image is recorded on a CID array solid state video camera in a 128 x 128 pixel format. The camera can be translated through the image field under computer control by stepping-motor driven precision translation stages. The irradiance data can be stored on a floppy disk and displayed as an image on a CRT. The irradiance data from each pixel can be directly addressed and analyzed by FORTRAN programming. An LSI 11/23 microcomputer is used for all control, recording and processing functions. The system permits one to calibrate the camera pixel by pixel, and the computer will then automatically adjust each irradiance value accordingly when recording data. A calibration scheme was formalized, and a technical manual for the system was written. The software and hardware for interfacing and controlling the camera, displaying an image and enabling processing of the data all were developed by graduate students under the sponsorship of this ARO contract.

3.1.2 Fringe Analysis

Interferograms of aerodynamic flows are likely to have two undesirable characteristics: They may be noisy, i.e. contain extraneous irradiance variations and laser speckle, and they often may contain regions in which fringes are few in number and therefore broad and difficult to interpret. Because the irradiance is accurately known at a large number of closely-spaced points in the field, we developed a fringe analysis scheme

to optimize the use of the data to produce accurate phase data even in the presence of considerable noise. The technique is based on the use of nonlinear regression analysis to fit irradiance data along a line to a curve of the form

$$I(x) = B(x) + E(x) \cdot \cos[P(x)],$$

where $B(x)$ represents the variation of background irradiance, $E(x)$ represents the envelope function of the fringes and $P(x)$ is the phase variation, i.e. $P(x)$ is the data needed for analysis of the density field. Although the approach is quite general, polynomials with unknown coefficients were used represent $B(x)$, $E(x)$ and $P(x)$ in most of our work. The nonlinear regression algorithm used was based on Powell's method.

Although the nonlinear regression analysis requires rather sophisticated programming and searching, the approach of curve fitting may appear somewhat old fashioned in comparison with digital filtering techniques; however, we used this approach because it recognizes that, physically, the fringe pattern must have an irradiance distribution of the form indicated above. We verified experimentally that the technique can be used to interpret extremely noisy interferograms with "subfringe" accuracy. The results of this investigation have been presented in a journal article referenced below.

3.2 Tomographic Algorithm Development

We considered two topics in the development of computer tomographic algorithms for analysis of holographic

interferograms. The first work deals with the effects of strong refraction and was only partially sponsored by this contract. The second deals with an new iterative convolution technique.

3.2.1 Reconstruction of Strongly Refracting Fields

This work is mentioned here briefly because much of it was carried out under different sponsorship; however, it was completed under this project and has strong relevance to it. Virtually all computer tomography algorithms are based on the assumption that the probing rays are straight lines through the unknown field so that the data represent line integrals. When a fluid under study by interferometry has strong density gradients, the assumption that the the rays are straight lines may not be reasonable. An example of such strong gradients would be a shock wave. We have developed a basic algorithm for dealing with this case. It involves an iterative process. An initial estimate of the field is made by reconstruction from the data without accounting for ray bending due to strong gradients. Path integrals through the estimated field are then computed by numerical ray tracing. The values of these path integrals are then compared with the measured experimental data. Based on the difference between the measured and calculated data, the estimate of the field is revised. This process continues iteratively until an acceptable reconstruction of the field is obtained. Details of this work are reported in a journal article referenced below.

3.2.2 The Iterative Convolution Method

Most well-established algorithms for computer tomography assume that data are complete. In this case "complete" means that projections (interferograms) are available over the entire 180° range of viewing directions, even though they may be available only at discrete intervals. "Complete" also means that no opaque objects are present in the field to block portions of the projections. Both of these conditions are likely to be violated in aerodynamic experiments. Physical constraints may make it impossible to view a region such as the test section of a wind tunnel from a complete range of viewing directions. Furthermore, an object such as the aerodynamic model under test is likely to block a substantial region of the field of interest. We therefore were particularly interested in developing algorithms that would work even when the data are incomplete in either of the senses noted above.

The most popular algorithm for tomographic reconstruction probably is the convolution backprojection algorithm (termed the convolution method here). The theory of operation of this algorithm is well understood, and it runs rapidly and efficiently on a computer and places relatively modest demands on storage. The basic reason for its simplicity of operation is that it operates in the object domain. Unfortunately, it requires that data be complete and available at equally spaced intervals; hence, it is not directly useful for the analysis of most aerodynamic data.

As part of this project we attempted to develop an algorithm that would retain many of the positive attributes of the

convolution method, but which could be used to analyze incomplete data from aerodynamic experiments. We were partially, but not completely, successful in this attempt.

The algorithm we developed is called the Iterative Convolution Method. It operates by iteration between the object and projection (Radon Transform) domains. It begins by examining the projections (fringe data) and filling in missing data according to some specified criteria. For example, the "artificial data" used to fill in missing projections can be formed to have known mathematical characteristics of Radon transforms, such as integrals which must be the same in each projection. Other constraints such as known bandlimits can also be applied at this stage. Once this has been done, the field can be reconstructed by the efficient convolution method. New projections are then computed as line integrals across this estimated reconstruction. Constraints such as finite spatial extent can be applied at this stage. These computed projections are replaced by measured values everywhere real data are available. A new reconstruction is then made by the convolution method and the process continues iteratively.

We have written several codes based on this general algorithm and have tested them with both simulated and actual experimental data. Our results were mixed. When data are incomplete because the entire range of viewing directions is not accessible, the algorithm did not produce reconstructions as accurate as those produced by other applicable methods based on series expansions of the unknown field. When data are incomplete

because an opaque object such as an aerodynamic test model blocks part of the projections, the algorithm appears to work reasonably well. It must be noted that this algorithm is nonlinear and is being used to obtain an approximate solution to a problem which is mathematically ill-posed. Its convergence behavior when the data is substantially incomplete is interesting. It generally converges toward an accurate reconstruction for several iterations and then diverges. We were able to empirically establish criteria for stopping the algorithm at, or very near, the iteration in which the most accurate estimate is produced.

After initial development and testing under this program, further work was done on this algorithm, including applying it to wind tunnel data by a post doctoral researcher sponsored by NASA. Details of the algorithm and an analysis of it are presented in a journal article currently under review.

3.3 Experimentation

We have been involved with experiments using holographic interferometry with analysis by computer tomography in three ways. First, a simple small scale experiment was carried out at an early stage to illustrate the principle. Second, we have been working toward conducting a low-speed wind tunnel experiment to measure the density distribution in a jet inserted into a cross flow. Third, we have maintained an active interest in, and discussion of, large-scale experiments being developed at Ames Research Center. The first two of these will be described briefly here.

3.3.1 Demonstration Experiment

At an early stage in this program we conducted a feasibility experiment to show that the technique could be used to reconstruct a density field that was geometrically similar to that anticipated in rotating aerodynamic fields such as the transonic flows near helicopter rotors. The actual test object was the temperature field above a curved heated wire mounted on a rotating table submerged in water. Data were recorded by holographic interferometry at each of several rotational positions of this object, as would be the case in an experiment in a rotating system. The data were then used to reconstruct the temperature field by using the convolution method described above. The results were qualitatively correct, and gave us confidence to proceed as planned.

3.3.2 Wind Tunnel Experimentation

Although we have made considerable progress toward conducting an in-house wind tunnel experiment, it was not brought to completion during this contract period. The problem we are working on is the insertion of a high-density gas jet into an orthogonal cross flow. The desired result is a mapping of the density distribution in crosssections of the jet as it bends and expands. This case has interest and relevance to problems such as injection cooling of turbine engines, and at the same time has many features in common with compressible aerodynamic flows. For example, it has been predicted that the jet will develop a double vortex structure as it bends.

We have decided to create the high-density jet by cooling a gas such as Carbon dioxide or Nitrogen to a low temperature. We have experimented with various systems for doing so, such as heat transfer from packed beds of dry ice or heat exchange with boiling liquid Nitrogen.

We have begun experimental work to record interferograms with a pulsed ruby laser, and have been working on a scheme to use reflection holography to record appropriate holograms in the confined test space around the tunnel. This work is continuing under a new ARO contract.

3.4 Hybrid Processor for Wavefront Recording

Although holography has many advantages over other techniques for making optical measurements of aerodynamic flows, it also has certain drawbacks, primarily based on the necessity to record two sequential exposures. Therefore there would be advantages to a technique that could accurately record quantitative data about an optical wavefront that has been distorted by passage through a flow without the need for two recordings. We therefore explored the use of hybrid processing, i.e. the combining of optical and computer processing of optical data.

The system we developed is based on the use of a simple, well-known technique of optical Fourier processing. The wave front to be studied enters a processor that consists of two lenses separated axially by the sum of their focal lengths. At the back focal plane of the first lens the resulting irradiance pattern is known to represent the Fourier transform of the

entering wave. In this transform plane we place a filter that differentiates the signal, i.e. the output of the second lens is the derivative of the input wave. This system is very similar to a classical schlieren system with laser illumination, except the filter is more complicated than a knife edge.

The output of the optical processor is recorded by a solid state array camera and stored in a computer where it is integrated to give the phase distribution across the field. This phase distribution is the information we normally would record by interferometry. The processing described so far is straightforward and well known. However, such coherent optical processing is notoriously noisy, so much so that it is not very useful for practical applications to flow visualization and measurement. We have developed a technique for greatly improving it. In our technique, the computer records three different outputs from the optical processor. Each corresponds in essence to a slightly different position of the filter in the Fourier plane. When these three signals are combined in a particular algebraic manner in the computer, most of the noise, including that caused by nonuniform background illumination and much of the speckle noise are eliminated. We believe that this hybrid processing technique is a potentially important flow diagnostic tool. This work is described in detail in a journal article referenced below.

4. PUBLICATIONS

4.1 Journal Articles

S. Cha and C. M. Vest, "Tomographic reconstruction of strongly refracting fields and its application to interferometric measurement of boundary layers", Applied Optics, 20, 2787-2794 (1981).

J. B. Schemm and C. M. Vest, "Fringe pattern recognition and interpolation using nonlinear regression analysis", Applied Optics, 22, 2850-2853 (1983).

I. Prikryl and C. M. Vest, "Hybrid processing for phase measurement in metrology and flow diagnostics", Applied Optics, 22, 2844-2849 (1983).

I. Prikryl and C. M. Vest, "Tomography by Iterative Convolution and its application to aerodynamic measurements", (In preparation; based in part on work carried out under this contract.)

4.2 Presentations at Technical Meetings

W. Braga, "Computer tomography by iteration between image and projection spaces", Annual meeting of the Optical Society of America, Kissimmee, Florida, October, 1981.

J. B. Schemm, "Fringe interpolation by nonlinear regression",
Annual meeting of the Optical Society of America, Tucson,
Arizona, October, 1982.

4.3 Reports

J. B. Schemm, "Users Manual and Technical Specifications of
Digital Camera System", Internal Report, Interferometry
Laboratory, Department of Mechanical Engineering and Applied
Mechanics, The University of Michigan, 147 pp (1983).

C. M. Vest, Progress Reports to ARO covering the following
periods:

20 October 1980 - 30 June 1981

1 July 1981 - 31 December 1981

1 January 1982 - 30 June 1982

1 July 1982 - 31 December 1982

1 January 1983 - 30 June 1983.

5. PARTICIPATING SCIENTIFIC PERSONNEL

Dr. C. M. Vest, Professor, principal investigator

Mr. Washington Braga, doctoral student

Mr. John B. Schemm, doctoral student

Mr. John Dec, doctoral student

Mr. John Kittleson, masters student; MSE awarded August 1981

Mr. Scott Lissitt, masters student; MSE awarded August 1983

Dr. Ivan Prikryl, Visiting Associate Research Scientist

Notes: Mr. Braga and Dr. Prikryl were primarily sponsored by other fellowships, but made significant contributions to this research program. Mr. Kittleson, as a direct result of his experience with this program, was hired by the U.S. Army Aeromechanics Laboratory at Moffet Field, CA to work on holographic instrumentation of aerodynamic experiments.

APPENDIX

This appendix contains copies of journal articles based on this research which have been published to date.

Hybrid processing for phase measurement in metrology and flow diagnostics

Ivan Prikryl and Charles M. Vest

A hybrid optical-digital processing scheme for measuring phase distributions is described and demonstrated. It is intended to be an alternative to interferometric methods of measuring optical path length changes in flow diagnostics and can also be used as a flow visualization technique. The processing scheme enables one to make accurate measurements of phase at arbitrary points in the image plane. The system is based on a simple coherent optical Fourier processor but incorporates three separate measurements and postdetection digital processing to eliminate extraneous parts of the signal. The addition of a holographic filter to the system enables one to measure deformation or displacement of diffusely reflecting opaque objects. The technique is demonstrated by using it to visualize the flow of an expanding compressible gas jet and to measure the optical path length through a heated plume of air.

I. Introduction

Many physical measurement techniques require the determination of the spatial distribution of phase of coherent light in some plane. Because detectors are not capable of responding at optical frequencies, phase distributions must be coded into irradiance distributions which can be detected or recorded by square-law detectors such as photosensors or photographic film. The most common technique for such encoding is interferometry, whereby the phase distribution is displayed as a fringe pattern. From such a pattern, relative phases at the center of fringes can be determined. However, when accurate measurements must be made at other points, such as on a uniform grid of points which do not coincide with fringe centers, additional effort is required. For example, a heterodyne system can be used,¹ or irradiance measurements at the points can be determined by interpolation.² This interpolation is not straightforward because the desired phase distribution is the argument of a fringe function, most often sinusoidal.

In automated systems, irradiance distributions can be recorded directly using vidicons or solid-state detector arrays, thus bypassing the intermediate step of photographing fringe patterns. In this paper we point

out that, when the capability of accurately and rapidly recording irradiance distributions exists, it may be desirable to reconsider other ways of mapping phase distributions into irradiance variations, namely, coherent optical Fourier processing and related filtered schlieren and shearing interferometric techniques. In particular, we discuss ways of recording phase gradients, which can be integrated, if necessary, to determine phase distributions. We first describe the approach in a form suitable for applications in which a plane object wave has been slightly distorted by passage through a transparent medium or reflected by a specular surface. This would be applicable to wind tunnel diagnostics, heat transfer studies, plasma diagnostics, etc. An extension of the technique will then be described in which a holographic filter can be used to measure phase differences due to distortion or motion of diffusely scattering surfaces.

II. Method

In the proposed method the phase distribution of a slightly distorted plane wave of coherent light is measured by passing the wave through a simple optical processor which performs a total differentiation. The output of the processor is recorded with a vidicon or solid-state array camera and subsequently analyzed further by a digital computer. It will be demonstrated that this hybrid approach alleviates many of the practical difficulties associated with coherent optical processing. Such a system is shown in Fig. 1.

Let

$$u(x,y) = a(x,y) \exp[i\phi(x,y)]$$

be the complex amplitude in a plane $z = \text{constant}$ of

The authors are with University of Michigan, Department of Mechanical Engineering & Applied Mechanics, Ann Arbor, Michigan 48109.

Received 7 February 1983.

0003-6935/83/182844-06\$01.00/0.

© 1983 Optical Society of America.

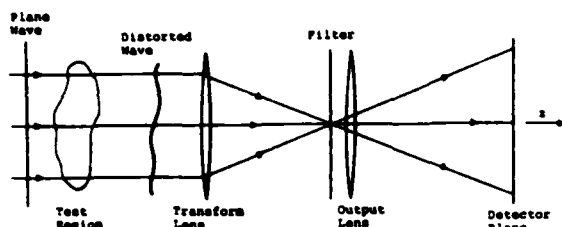


Fig. 1. Optical processor. The filter is placed in the back focal plane of the transforming lens. In general, the output lens is aligned to form an image of the test region in the detector plane.

interest. Our objective is to determine $\phi(x,y)$. As shown in Fig. 1, the processor consists of a Fourier transforming lens, a Fourier filter in its back focal plane, and a second lens which reforms the processed wave front so that its irradiance distribution can be recorded photographically or electronically. The Fourier filter used in the current study is designed so that the processor forms the total differential of the input signal.

Now suppose that the filter that performs the differential operation is translated laterally (parallel to the X axis) a distance $-\epsilon f/k$, where f is the focal length of the transforming lens and $k = 2\pi/\lambda$ is the wave number. The translated filter will differentiate the function

$$u(X,Y) = g(X,Y) \exp[i\phi(X,Y) + i\epsilon X] \quad (2)$$

instead of the function (1) and simultaneously will multiply the differential by the value $\exp(-i\epsilon X)$. The output of the processor will be

$$du(X,Y) = [dg(X,Y) + ig(X,Y)[d\phi(X,Y) + \epsilon dX]] \cdot \exp[i\phi(X,Y)] \quad (3)$$

where

$$dg(X,Y) = \frac{\partial g(X,Y)}{\partial X} dX + \frac{\partial g(X,Y)}{\partial Y} dY \quad (4)$$

$$d\phi(X,Y) = \frac{\partial \phi(X,Y)}{\partial X} dX + \frac{\partial \phi(X,Y)}{\partial Y} dY \quad (5)$$

The irradiance distribution of the output would be

$$I(X,Y) = [dg(X,Y)]^2 + g^2(X,Y)[d\phi(X,Y) + \epsilon dX]^2 \quad (6)$$

This irradiance distribution is recorded electronically and stored in the memory of a digital computer for subsequent additional processing.

The total differential $d\phi(X,Y)$ which we desire to measure is present in this expression for the irradiance $I(X,Y)$ but must be separated from the effects of $g^2(X,Y)$ and $[dg(X,Y)]^2$. Such a separation can be made if three different irradiance measurements are made, each corresponding to a different position of the filter. In particular, let the measurements $I_0(X,Y)$, $I_1(X,Y)$, and $I_2(X,Y)$ correspond to values $\epsilon = 0$, $\epsilon = -\epsilon_0$, and $\epsilon = \epsilon_0$, respectively. From Eq. (6) it is easily shown that

$$d\phi(X,Y) = \frac{1}{2}(\epsilon_0 dX) \frac{I_2(X,Y) - I_0(X,Y)}{I_0(X,Y) + I_2(X,Y) - 2I_1(X,Y)} \quad (7)$$

Note that the denominator of Eq. (7) equals $2g^2(X,Y)\epsilon_0^2(dX)^2$ which is nonzero as long as $g(X,Y)$ and ϵ_0 are

nonzero. We note that the use of three measurements to remove ambiguity and to remove extraneous components of the irradiance distribution is conceptually similar to certain techniques of two-reference beam holographic interferometry,³ real-time holographic interferometry,⁴ and interferometric real-time phase measurement.⁵

Having determined the total differential $d\phi(X,Y)$ over the $X-Y$ plane by using Eq. (7), the phase $\phi(P)$ at any point P can be found by path integration along any curve which connects P and any point P_0 where the phase has a known value $\phi(P_0)$:

$$\phi(P) = \int_{P_0}^P d\phi(P) + \phi(P_0) \quad (8)$$

Such integration of optically differentiated phase distributions has been reported by Sprague and Thompson⁶ who used an optical integration technique.

If the wave front under consideration contains an aberration $\phi_n(X,Y)$ whose order does not exceed that of the variation $\phi(X,Y)$ under study the technique can still be used. In this case the complex amplitude Eq. (1) contains the $\phi(X,Y) + \phi_n(X,Y)$ as its phase term, where $\phi_n(X,Y)$ may be due to misalignment, imperfect optical elements, or low quality test section windows. If $\phi_n(X,Y)$ does not change with time, two sets of three exposures can be recorded—one set before the change $\phi(X,Y)$ is introduced and one set after it is. Because the computed phases are stored in a computer, they can be subtracted to give information only about $\phi(X,Y)$. This is illustrated experimentally in Sec. IV.

III. Differential Filters

We mention here two types of filter which could be used in the optical processor described in the previous section. The first is the ideal Fourier filter for forming a differential, and the second is a composite grating that approximates the desired filter.

The ideal filter to perform a differentiation is based on the differentiation theorem of Fourier transforms.

$$\begin{aligned} \partial f(X,Y) / \partial X &= iuF(u,v) \\ \partial f(X,Y) / \partial Y &= vF(u,v) \end{aligned} \quad (9)$$

where $F(u,v) = \mathcal{F}\{f(X,Y)\}$ is the 2-D Fourier transform of $f(X,Y)$. For our purposes, $f(X,Y)$ represents the complex amplitude of the input field to the processor. The first lens of the processor produces the Fourier transform of this field in its back focal plane. If ξ and η are the physical coordinates in this plane, the complex amplitude there is

$$F[k\xi/f, k\eta/f] \quad (10)$$

where $k = 2\pi/\lambda$ and f is the focal length of the transforming lens.

According to Eqs. (9) the filter must have an amplitude transmittance which varies linearly in the transform plane and must produce a phase shift to simulate negative values of u and v . Hence the filter must have the following intensity transmittance:

$$T(k\xi/f, k\eta/f) = C^2(k\xi/f + k\eta/f)^2 \quad (11)$$

and have a $\lambda/2$ thin film layer in the region $(k/f)(\xi + \eta) < 0$ in order to introduce the phase shift π :

$$n = \begin{cases} 0 & \text{for } (k/f)(\xi + \eta) \geq 0, \\ \pi & \text{for } (k/f)(\xi + \eta) < 0. \end{cases} \quad (12)$$

The constant C should have a value such that the intensity transmittance is unity at the outer edge of the filter:

$$C^2(k\xi f + k\eta f)\epsilon_{max} = 1. \quad (13)$$

The processor using this filter will produce a single output wave of the form of Eq. (3) where the parameters in Eqs. (3)–(5) must be interpreted as follows:

$$u(X, Y) = C[u_0(X, Y) + u_1(X, Y) + u_2(X, Y)], \quad (14)$$

$$dX = -C,$$

$$dY = -C.$$

Then Eqs. (6) and (7) are also valid if we take

$$(dX)^2 = (dY)^2 = (dX dY) = C^2. \quad (15)$$

One possible realization of the ideal filter for 1-D differentiation has been used by Cody⁷ to visualize gradients in compressible flows. In his experiments two separate filters were used—one with a quadratic intensity transmittance and one with a step change of phase. These filters were placed at conjugate planes of an additional lens in the processor.

Other ways of forming differentials without using a $\lambda/2$ thin film have been investigated. Usually some compensation must be used to correct for nonlinear relationships between the detected irradiance and the derivative of the phase. This compensation may involve heavy postdetection electronic processing,⁸ strong predetection biasing,⁹ or the use of a square root filter rather than a linear filter.⁹

A composite grating can be used as a Fourier filter to perform the operation in Eq. (3) on a more approximate basis.¹⁰ An appropriate composite grating can be produced very easily, and one was used in the illustrative experiments described in Sec. IV.

We first consider a composite grating filter which performs an approximate differentiation in one dimension. It consists of two superimposed sinusoidal gratings which have slightly different frequencies and which are shifted by half a period relative to each other. Each grating will produce three component waves in the Fourier plane—the central order and two diffracted orders. The propagation angle of the diffracted waves is proportional to the grating frequency. Hence each diffracted order leaving the composite grating will contain a pair of waves having slightly different propagation directions and a relative phase shift of π . Correspondingly, in the output (inverse Fourier transform) plane each order will consist of two slightly sheared and shifted waves. Hence the processor with this filter acts as a modified shearing interferometer. If T is the period of one grating and the period of the other grating is $T + \Delta T$, the shear will be

$$\Delta X = \lambda f (\Delta T / T), \quad (16)$$

where f is the focal length of the first lens of the processor.

Stated differently, the impulse response of the processor is

$$\delta(X + \Delta X, Y) - \delta(X, Y), \quad (17)$$

where δ is the Dirac delta function. (In this discussion we assume that the origin of the coordinate system has been shifted to the center of one of the diffracted orders.) So, if $u(X, Y)$ is the input signal, the output is

$$u(X + \Delta X, Y) - u(X, Y). \quad (18)$$

If ΔX is sufficiently small to express the difference in Eq. (18) using only the first two terms of a Taylor series, we see that the output is approximately

$$-\partial u / \partial X \Delta X. \quad (19)$$

If the wave having complex amplitude $u(X, Y)$ given by Eq. (2) is acted on by this processor, the output will be

$$\begin{aligned} \Delta u(X, Y) = & \left[\left[u(X, Y) + \frac{\partial u}{\partial X} \Delta X \right] \right. \\ & \times \exp \left[i \left(\frac{\partial \phi}{\partial X} \Delta X + \epsilon \Delta X \right) \right] - u(X, Y) \left. \right] \\ & \times \exp[i\phi(X, Y)]. \end{aligned} \quad (20)$$

The corresponding irradiance distribution is

$$\begin{aligned} I(X, Y) = & \left[u(X, Y) + \frac{\partial u}{\partial X} \Delta X \right]^2 \\ & - 2u(X, Y) \left[u(X, Y) + \frac{\partial u}{\partial X} \Delta X \right] \\ & \times \cos \left(\frac{\partial \phi}{\partial X} \Delta X + \epsilon \Delta X \right). \end{aligned} \quad (21)$$

Finally, if the operation described in Sec. II were carried out, the expression corresponding to Eq. (7) would be

$$\tan \left(\frac{\partial \phi}{\partial X} \Delta X \right) = \frac{1 - \cos(\epsilon \Delta X)}{\sin(\epsilon \Delta X)} \frac{I_0(X, Y) - I_1(X, Y)}{I_0(X, Y) + I_1(X, Y) - 2I_2(X, Y)},$$

Hence if ΔX and $\epsilon \Delta X$ are sufficiently small, then

$$\frac{\partial \phi(X, Y)}{\partial X} \Delta X = \frac{1}{2} \epsilon \Delta X \frac{I_0(X, Y) - I_1(X, Y)}{I_0(X, Y) + I_1(X, Y) - 2I_2(X, Y)},$$

which is of the desired form (in one dimension). In particular, ΔX must be small enough so that

$$|\tan(\epsilon \Delta X)| \leq \epsilon \Delta X \quad (22)$$

throughout the field for Eq. (23) to be valid.

As would be expected on physical grounds, Eq. (22) will be unambiguous only if

$$-\pi/2 < \frac{\partial \phi}{\partial X} \Delta X < \pi/2. \quad (23)$$

Hence

$$\Delta X < \pi/2 \left(\left| \frac{\partial \phi}{\partial X} \right| \right)^{-1} \quad (24)$$

is a criterion which must be met by the processor in order to use Eq. (22). Analysis also indicates that the angle ϵ in Eq. (22) must be chosen such that

$$0 < \Delta X < \pi. \quad (27)$$

Preferably, the value of $\epsilon_0 \Delta X$ should be chosen to be $\pi/2$. If simultaneously we choose a value of ΔX close to the limit in Eq. (26), we obtain the maximum possible difference between the intensities I_2 and I_1 . This difference varies from zero (for $d\phi = 0$) to the maximum intensity which can be reached by constructive interference in the instrument. The best value for ϵ_0 is

$$\epsilon_0 = |\phi(\phi(X))|_{\max}. \quad (28)$$

To form an approximate total differential as required in Eq. (7), the composite grating can consist of three sinusoidal amplitude gratings which yield the impulse response¹⁰

$$\phi(X + \Delta X, Y) + \phi(X, Y + \Delta Y) - 2\phi(X, Y). \quad (29)$$

This filter will be subject to restrictions analogous to Eq. (24). Also, the radius R of the filter, which should also be the aperture stop of the processor, is such that

$$\sin(R/f) \gg R/f \gg \lambda/2(\Delta X + \Delta Y) \gg \lambda, \quad (30)$$

where f is the focal length of the transforming lens. Condition (30) permits the impulse response to be approximated by delta functions as in Eq. (29).

Note that if composite grating filters are used they must be designed so that in a given experiment ΔX and ΔY will meet the criteria which depend on the maximum value of the phase distribution $\phi(X, Y)$.

IV. Experimental Results

Two experiments were conducted in order to demonstrate this technique. In the first, the optical processor was used to visualize a compressible gas jet. In the second, the hybrid processor was used to measure the temperature-dependent optical path length distribution across a natural convective plume. In the latter case the ability to remove the effects of wave front aberrations was also demonstrated.

Both experiments were carried out using a composite grating filter constructed by recording interference patterns on a holographic plate. The grating performed an approximate 1-D differential operation. It produced a background wave and two composite diffracted waves traveling at angles of $\pm 15^\circ$ with respect to the z axis and having linear shears $\Delta X = 0.2$ mm in object space. The impulse response of either off-axis component is given by Eq. (17).

In the first experiment the object was a jet of compressed nitrogen gas flowing from a nozzle. In this case the output of the optical processor was recorded photographically. Figure 2 is a photograph of the nozzle with no flow. Note the bright lines which form because of the steep horizontal gradients in the image at the vertical edges of the nozzle. The width of these lines is defined by the shear $\Delta X = 0.2$ mm. Figure 3 is a photograph recorded while the gas jet was present. The edges of the jet and its periodic structure are clearly visible.

In the second experiment the output of the optical processor was recorded by using a solid-state CID array

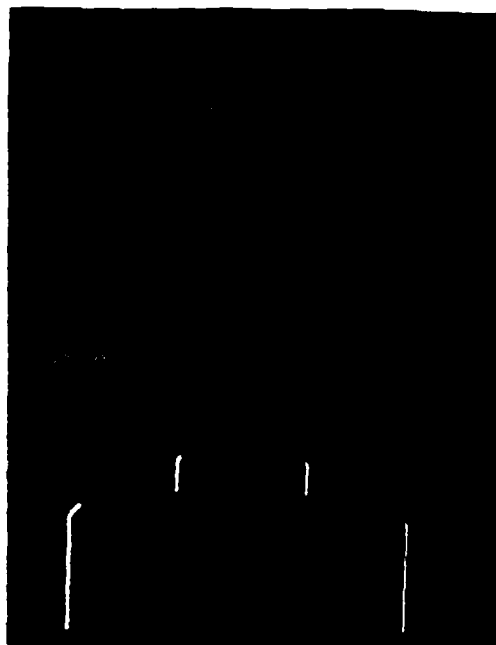


Fig. 2. Processed image of a nozzle with no flow.



Fig. 3. Processed image of a jet of nitrogen gas flowing from a nozzle. A composite grating filter is used to differentiate approximately in the horizontal direction.

camera with 128×128 pixels. The images recorded by the camera were stored in and processed by a microcomputer. The processing consisted of two parts. First, each signal was averaged over a few pixels in the vertical direction to suppress noise introduced by the photographic grating. Second, after the three required images were recorded, Eq. (22) was evaluated. Finally,

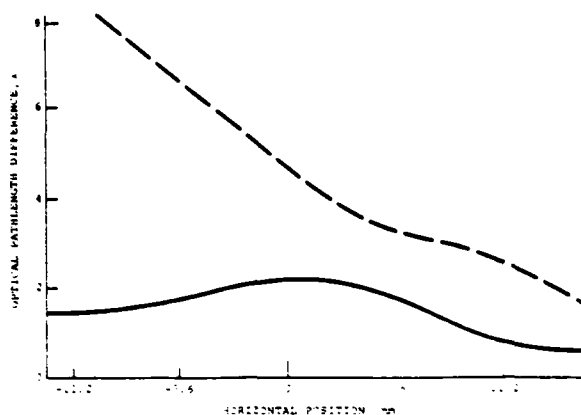


Fig. 4. Measured optical path length distributions across a heated plume of air. The dashed curve includes the effect of wave front tilt. The solid curve is the corrected distribution after wave front tilt has been removed.

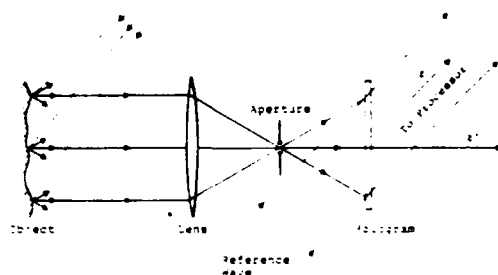


Fig. 5. Holographic system used when the object wave is tilted. The lens images the object onto the recording plane.

the resulting values of the path length gradients were integrated to obtain values of the path length itself. Two sets of measurements were made in this way and were subtracted to give the desired phase distribution.

The light wave was tilted slightly in order to introduce an extraneous phase shift which was considered to be noise in the signal. Figure 4 is a plot of the optical path length distribution measured in this way. The dashed curve is the optical path length distribution due to the sum of the noise and the heated plume. The solid curve is the distribution after the noise was filtered out by subtracting the measurement made without the heated plume from that made with the plume.

V. Application to Complicated or Diffuse Waves

In Secs. II-IV we have considered the application of a hybrid processor to measure the phase distribution of a relatively simple wave front, e.g., a plane wave which has traveled through a wind tunnel test section or has been distorted slightly by a reflective or refractive optical element. If the wave of interest is diffused prior to passing through a transparent object or is scattered by a diffuse opaque object whose deformation is to be measured, the system can be used if a holographic filter is added to it.

The required holographic system is shown in Fig. 5. The diffuse object surface is imaged onto a recording medium. In the recording plane $z' = 0$, the complex amplitude of the object wave is

$$u_o(x', y') = a_o \exp[i\Phi(x', y')] \quad (31)$$

An off-axis image plane hologram is recorded by adding to $u_o(x', y')$ a reference wave

$$u_R(x', y') = a_R \exp[i(\alpha x' + \gamma z')] \quad (32)$$

This hologram is developed in place or is developed and precisely replaced in the system after development. It has an amplitude transmittance of the form

$$t_h = t_0(x', y') + \beta \exp[i\Phi(x', y') - \alpha x'] + \exp[-i\Phi(x', y') - \alpha x'] \quad (33)$$

The disturbance of interest is then introduced so that the object wave at the hologram plane becomes

$$u_o(x', y') = a_o \exp[i\Phi(x', y') + \phi(x', y')] \quad (34)$$

where the distribution of phase change $\phi(x', y')$ is the quantity to be measured.

If $u_o(x', y')$ alone illuminates the hologram described by Eq. (33), the output of the hologram will be

$$u_o(x', y') t_h(x', y') = a_o \exp[i\Phi + \phi] + \beta \exp[i2\Phi + \phi - \alpha x'] + \beta \exp[i\phi + \alpha x'] \quad (35)$$

Equation (35) indicates that the wave traveling away from the hologram in the same direction as the original reference wave has the desired phase structure and can serve as the input wave for the hybrid processor (see Fig. 5). The complicated phase structure $\Phi(x', y')$, which remains constant between exposures, has been removed from this wave. Note that, if the z axis of the coordinate system used in writing Eq. (1) is taken to be in the propagation direction of the holographic reference wave (32), the last term in Eq. (35) is identical to that in Eq. (1) with

$$u_o(x', y') = a_o \exp[i\phi(x', y')]$$

If the motion or phase disturbance creates a system of fringes localized off the surface of the object under study, the imaging system should be focused on the region of localization and/or the aperture must be sufficiently small to form a well-defined structure of phase difference $\phi(x', y')$ in the hologram plane. By placing the aperture stop in the focal plane of the imaging lens it can be insured that the surface of localization is on the object surface.

If necessary, the wave leaving the holographic filter can be recorded at any instant of time on a second off-axis hologram. This wave can be reconstructed at any later time and processed.

VI. Conclusion

In summary, we have described and demonstrated techniques for using hybrid processing to visualize and measure phase changes due to variations of refractive index in transparent media or deformation or displacement of opaque objects. Potential advantages of

this technique relative to interferometry include the ability to make accurate phase measurements at arbitrary points (not just at fringe centers) and the ability to make such measurements without ambiguity in sign of phase change. The technique uses digital processing to remove much of the optical noise associated with coherent optical processing.

The authors wish to acknowledge the assistance of John B. Schemm who developed the camera/computer system used to perform the digital processing. This work was sponsored by the U.S. Army Research Office.

References

1. R. Dandliker, *Prog. Opt.* 17, 1 (1980).
2. J. B. Schemm and C. M. Vest, *Appl. Opt.* 22, 2850 (1983).
3. R. Dandliker, R. Thalmann, and N. Brown, *Opt. Commun.* 42, 301 (1982).
4. P. Hariharan, B. F. Oreb, and N. Brown, *Opt. Commun.* 41, 393 (1982).
5. L. M. Frantz, A. A. Sawchuk, and W. von der Ohe, *Appl. Opt.* 18, 3301 (1979).
6. R. A. Sprague and B. J. Thompson, *Appl. Opt.* 11, 1469 (1972).
7. R. L. Cody, "A Comparison of Various Coherent Optical Filtering Operations," M.S. Thesis, U. Tennessee (1971).
8. D. Kermisch, *J. Op. Soc. Am.* 65, 887 (1975).
9. B. A. Horwitz, *Opt. Commun.* 17, 231 (1976).
10. S. H. Lee, in *Optical Information Processing Fundamentals*, S. H. Lee, Ed. (Springer, Berlin, 1981), pp. 45-50.
11. I. Prikyl, *Opt. Acta* 21, 675 (1974).

Fringe pattern recognition and interpolation using nonlinear regression analysis

John B. Schemm and Charles M. Vest

Least-square error criteria are used to fit 1-D interference fringe pattern irradiance data to a physically meaningful function of the form $I(x) = B(x) + E(x) \cos[P(x)]$, where $B(x)$, $E(x)$, and $P(x)$ are low-order polynomials. This procedure is intended to complement digital fringe recognition by providing a method for smoothing and interpolating among fringe position data when the number of fringes is small, there are more than ten irradiance measurements per fringe, and accurate phase values are needed at arbitrary locations in the field.

I. Introduction

Accurate digital recognition and interpolation of interference fringe patterns in the presence of laser speckle and extraneous slowly varying background irradiance are important for development of automated systems for interpreting interferograms. The information of interest for quantitative analysis of an interferogram is the phase distribution encoded in the fringes or a derivative of this phase at arbitrary positions within the fringe pattern. If fringe spacing is large, it is necessary to interpolate among fringe position data to find this phase or its derivatives at such arbitrary positions. It is frequently necessary to smooth the fringe position data (particularly if there is noise such as speckle) to achieve accurate results. In this paper we present a method for performing this smoothing and interpolation that is intended to complement digital fringe recognition.

Fringe recognition generally involves locating the centers of dark and light fringes. Recently, various researchers have developed schemes to automate this process. Video or solid state array cameras provide irradiance measurements on a matrix of points (pixels) over the interferogram. Image enhancement, level slicing, edge detection, and related processing techniques are then used to locate fringe centers and to track them along continuous fringes (see e.g., Ref. 1).

The authors and their colleagues frequently work with holographic interferometry of transparent media. In this work, and in many other applications of interferometry, the number of fringes in a pattern may be very small. In such cases there is frequently not enough information for accurate evaluation of the phase distribution. There are not enough fringe centers, and their positions are not known with sufficient accuracy.

However, each individual irradiance measurement carries information about the phase of the fringe at its position. The method reported in this paper uses all the information available in the irradiance measurements to smooth and interpolate the phase of the fringes accurately. This is accomplished by using nonlinear regression analysis to fit an algebraic expression to the full irradiance field.

To develop this technique, 1-D fringe patterns were digitized as sets of values of irradiance measured at equally spaced intervals. Least-square error criteria were used to fit these measured values to a function of the form

$$I(x) = B(x) + E(x) \cos[P(x)], \quad (1)$$

where $B(x)$, $E(x)$, and $P(x)$ are low-order polynomials. $B(x)$ describes the variation of the background irradiance due to such things as nonuniform object illumination. $E(x)$ is an envelope function related to the visibility of the fringes. $P(x)$ is the phase of the fringes and is usually the quantity of interest.

This method is intended to circumvent some of the problems encountered by most fringe recognition schemes due to the undesirable characteristics of irradiance measurements. Two particular problems are noise and nonuniform illumination. Noise may be due to laser speckle or thermal and electrical effects in the sensor system. Fringe brightness and visibility may vary across the image because of fringe localization, nonuniform object illumination or reflectivity, a nonuniform holographic reference wave, a nonuniform holographic reconstruction wave, or any combination of them.

II. Discussion

Automated fringe pattern recognition systems have tended to copy the operation of the eye. Such systems recognize fringes and represent them in binary form as bright or dark regions. Variations in brightness and visibility generally are ignored. This makes accurate estimates of the phase distribution across fringes difficult.

The authors are with University of Michigan, Department of Mechanical Engineering & Applied Mechanics, Ann Arbor, Michigan 48109.

Received 8 April 1983.

0001-6935/83/182850-04\$01.00/0.

© 1983 Optical Society of America.

When two monochromatic linearly polarized wave fronts with complex amplitudes U_1 and U_2 ,

$$U_1(x) = A_1(x) \exp[-i\phi_1(x)], \quad (2)$$

$$U_2(x) = A_2(x) \exp[-i\phi_2(x)], \quad (3)$$

interfere, the irradiance $I(x)$ along a line through the field

$$I(x) = |U(x)|^2 = |U_1(x) + U_2(x)|^2 \quad (4)$$

has the form of Eq. (1). When one is describing the form of interference fringes it is common to assume that $B(x)$, the background irradiance, and $E(x)$, the envelope function, are constant and equal. This is not a reasonable assumption for automated digital processing of interference fringes.

Computerized video systems measure irradiance I_i at a large number of positions x_i . The irradiance measurements I_i have optical and electrical noise that make it difficult to evaluate the phase of interference fringes directly from them. In our approach an algebraic expression $\hat{I}(x_i)$ is fitted to the set of irradiance measurements by least-square error methods. A physically meaningful form for $\hat{I}(x_i)$,

$$\hat{I}(x_i) = B(x_i) + E(x_i) \cos[\hat{P}(x_i)], \quad (5)$$

has been used with low-order polynomials for $\hat{B}(x_i)$, $\hat{E}(x_i)$, and $\hat{P}(x_i)$. If e_i is the difference between an irradiance measurement and its fitted value,

$$e_i = I(x_i) - \hat{I}(x_i), \quad (6)$$

and the sum of the squares of the errors is denoted by E ,

$$E = \sum e_i^2, \quad (7)$$

the coefficients in the estimate $\hat{I}(x_i)$ are selected to minimize E .

In this manner the phase function $P(x)$ is approximated by the function $\hat{P}(x_i)$ with the constraint that $\hat{I}(x_i)$ describes the modulated cosine fringe function expected on physical grounds. The phase function is then available for interpolation, calculating derivatives, or any other type of evaluation.

III. Difficulties

The two major drawbacks of this method are both related to use of nonlinear regression analysis and suggest that it must be applied with great care. All nonlinear regression algorithms are iterative. As such they require significant amounts of computer time. Also, unlike linear regression analysis, they require initial guesses of the values of all coefficients.

Nonlinear regression analysis algorithms converge to the local minima of E nearest the initial guess. This may not be the correct solution. In the present application the irradiance estimate is sufficiently nonlinear that there can be a large number of these local minima. For the procedure to converge to the correct description of the fringe pattern the algorithm must have very good quality initial guesses.

Good initial guesses can be made by using a fringe recognition scheme to locate approximately the position and magnitude of the fringe maxima and minima. The fringe-order number can then be fitted to these positions using linear regression analysis. This provides an initial guess for the phase function estimate $\hat{P}(x_i)$. Linear regression analysis may also be used with the position and magnitude of the fringe maxima and minima to find initial guesses for the background and envelope function estimates $\hat{B}(x_i)$ and $\hat{E}(x_i)$, respectively.

Many nonlinear regression analysis algorithms are based on linearization of the problem in a local area. Although an extensive evaluation of different algorithms has not been made, we found that a Gauss-Newton (linearization) method from the IBM SSP package failed to converge to a valid solution in tests with fringe data. It seems that the irradiance distribution may be sufficiently nonlinear that algorithms based on linearization are not useful. An optimized iterative search technique suggested by Powell² has been used successfully. It is described in some detail in the Appendix.

IV. Example

Here we present an example which demonstrates the evaluation of a double-exposure holographic interferogram of a simply loaded aluminum beam. A system of lenses was used to form a full size real image of the aluminum beam from the reconstructed holographic image. A microcomputer was used to record irradiance measurements from a photometer connected to a 60- μ m fiber-optic probe. The probe scanned a 1-cm straight path in the plane of the real image of the beam. There were 197 irradiance measurements taken at approximately uniform intervals along the path.

The particular data set presented here is for a region which includes the maximum deflection of the beam. The fringes are not localized near the surface of the beam. Fringes to the left of the maximum deflection are localized behind the surface of the beam. Fringes to the right are localized in front of the beam. The imaging system used a small entrance pupil so that the fringes on both sides of the image are visible. This introduced a large amount of speckle noise into the image. Figure 1 shows the measured irradiance data for this image.

The positions of fringe centers (both maxima and minima) were estimated visually from Fig. 1. The position irradiance and relative phase at the fringe centers are listed in Table I. Linear regression analysis was used to fit a third-order polynomial to describe the phase of the fringes as a function of position. This provided the initial guesses for the phase function:

$$\hat{P}(x_i) = 2.80 + 31.0x - 27.9x^2 + 2.83x^3, \quad (8)$$

Figure 2 shows a plot of this initial guess phase distribution together with the fitted points.

To estimate the background and envelope functions, a straight line was fitted through the irradiance of the left and right fringe maxima to describe the amplitude

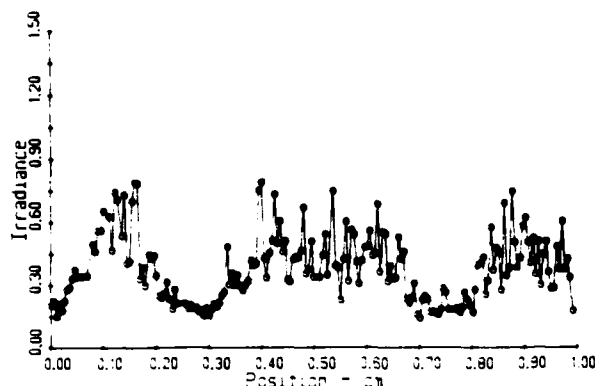


Fig. 1. Measured irradiance vs position for the fringe pattern evaluated in the example.

Table 1. Irradiance in Arbitrary Units and Phase in Radians at Fringe Centers

Position	Irradiance	Phase
0.01	0.20	3.142
0.13	0.62	6.283
0.29	0.17	9.425
0.50	0.50	?
0.73	0.19	9.425
0.89	0.51	6.283

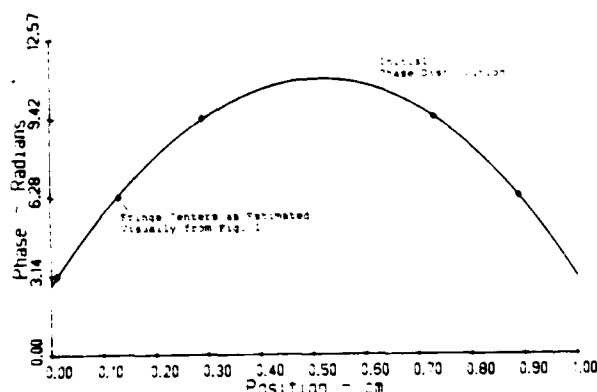


Fig. 2. Initial guess for the fringe pattern phase distribution. A third-order polynomial was fitted to the fringe centers by linear regression analysis. The coefficients from this curve fit are used as the initial guess for the nonlinear regression analysis.

of the maximum irradiance. Another straight line was fitted through the irradiance at the three fringe minima to describe the amplitude of the minimum irradiance. The average of the polynomials that describe the maximum and the minimum provide an initial guess for the background function:

$$B(x_i) = 0.414 - 0.0689x_i \quad (9)$$

Half of the difference between the maximum and the minimum is the initial guess for the envelope function:

$$\hat{E}(x_i) = 0.228 - 0.0753x_i \quad (10)$$

With these values as initial guesses, an iterative nonlinear regression analysis algorithm was used to

select the set of coefficients that yield the minimum sum of errors squared. Figure 3 shows the irradiance distribution that resulted from this process superimposed on the original irradiance data.

The phase function as determined by the nonlinear regression analysis is

$$\hat{P}(x_i) = 2.46 + 36.2x_i - 37.9x_i^2 + 1.99x_i^3 \quad (11)$$

Figure 4 shows this phase function from the nonlinear regression analysis compared with the initial guess phase function from analysis of fringe center positions. The maximum difference between the two estimates is $\pi/3$ rad.

In conventional fringe recognition, fringes are considered to be binary—they are either bright or dark. Using this convention, the center fringe in this example, which represents the maximum deflection of the beam, is considered a bright fringe. Our method based on nonlinear regression analysis is capable of recognizing that only a fractional fringe shift has occurred.

In this example application, as well as others we have studied, the numerical values of the sums of squared errors indicate that nonlinear regression significantly improves the description of the phase distribution over the initial guess. The initial guess irradiance description has a sum of squared errors of $E = 3.15$. If the background and envelope functions $\hat{B}(x_i)$ and $\hat{E}(x_i)$ are optimized by regression analysis while the phase function $\hat{P}(x_i)$ retains its initial guess values, the sum of

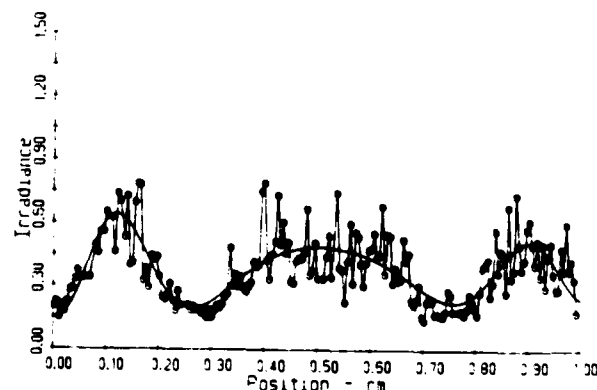


Fig. 3. Irradiance distribution function that resulted from the nonlinear regression analysis superimposed on the measured irradiance data.

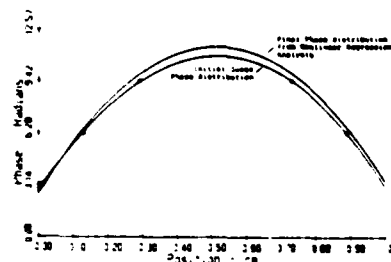


Fig. 4. Fringe pattern phase function that resulted from the nonlinear regression analysis compared with the initial guess phase function that was based on fringe center position data.

squared errors is reduced to $E = 2.71$. After optimization of the full irradiance description the sum of squared errors is reduced to $E = 2.13$.

V. Applicability

Evaluation of the fringe pattern described in this example and several other 1-D fringe patterns has led to some understanding of when this method will and will not contribute to evaluation of a fringe pattern. This method is most useful when there are only a few fringes in the image and when there are many irradiance measurements per fringe.

If there are more than a few fringes in a fringe pattern, there is probably sufficient information in the fringe position data to allow accurate evaluation of the phase function. However, even in a fringe pattern with many fringes it may be desirable to use this method in local sections of the fringe pattern, particularly if the data are noisy.

If there are only a few irradiance measurements per fringe, the information content of all the irradiance measurements may not be much greater than the information content of the fringe position data. In this case regression analysis will not provide a significantly more accurate estimate of the fringe phase.

For simple fringe patterns like the one in this example, with 200 or fewer data points and 10 or fewer coefficients, an LSI 11/23 microcomputer has been used to perform the calculations for this method. More complex problems have required use of a larger and faster computer.

In closing, we note that a variety of other techniques have been suggested for determining phase distributions from fringe data. The work of Brandt and Taylor is of particular relevance as it deals with problems of the type discussed in the present paper through an iterative technique to fit spline functions.^{3,4} Sollid⁵ fitted 2-D surface deformation patterns to Bezier polynomials. A referee has pointed out that several schemes based on linear regression analysis have been developed for interferometric testing of optical elements.⁶⁻⁸

Appendix: Numerical Method

We solved for all the coefficients in $\hat{B}(x_i)$, $\hat{E}(x_i)$, and $\hat{P}(x_i)$ using a nonlinear regression analysis algorithm proposed by Powell.² Powell's algorithm is an optimized version of a type in which one variable at a time is changed.

Consider the coefficients of $\hat{B}(x_i)$, $\hat{E}(x_i)$, and $\hat{P}(x_i)$ to be renamed as n coefficients x_r of the sum of squares of errors function E . The object of regression analysis is to find the values of the n parameters x_1, x_2, \dots, x_n so that the value of the sum of squares of errors $E(x_1, x_2, \dots, x_n)$ is a minimum. Consider x_1, x_2, \dots, x_n to be directions in an n -D space. These directions are probably not the optimum ones in which to search for the minimum of E . Powell describes a method and rationale for selecting vector combinations of parameter

directions that can be expected to be better for searching for the minimum of E . He also provides a criterion for selecting which search direction to replace with a new search direction and a criterion for deciding whether to actually make the replacement.

An iteration of Powell's algorithm starting from point \mathbf{p}_0 consists of the following five steps:

Step 1: A search along n direction vectors \mathbf{X} . For $r = 1, 2, \dots, n$ calculate λ_r so that $E(\mathbf{p}_{r-1} + \lambda_r \mathbf{X}_r)$ is a minimum and define $\mathbf{p}_r = \mathbf{p}_{r-1} + \lambda_r \mathbf{X}_r$.

Step 2: Determine which search gave the largest reduction in E . Find the integer m , $1 \leq m \leq n$, so that $[E(\mathbf{p}_{m-1}) - E(\mathbf{p}_m)]$ is a maximum, and define $\Delta = [E(\mathbf{p}_{m-1}) - E(\mathbf{p}_m)]$.

Step 3: Calculate $E_3 = E(2\mathbf{p}_n - \mathbf{p}_0)$ and define $E_1 = E(\mathbf{p}_0)$ and $E_2 = E(\mathbf{p}_n)$.

Step 4: Determine whether to replace the vector \mathbf{X}_m with a new vector. If $E_3 \geq E_1$ and/or $(E_1 - 2E_2 + E_3) \cdot (E_1 - E_2 - \Delta)^2 \geq -(E_1 - E_3)^2/2$, use the old directions $\mathbf{X}_1, \mathbf{X}_2, \dots, \mathbf{X}_m$ for the next iteration and use \mathbf{p}_n for the next \mathbf{p}_0 otherwise.

Step 5: Calculate the direction for a new vector \mathbf{X} . Define $\mathbf{X} = (\mathbf{p}_n - \mathbf{p}_0)$. Search along this new vector for the new minimum. Calculate λ so that $E(\mathbf{p}_n + \lambda \mathbf{X})$ is a minimum. Replace the vector \mathbf{X}_m with $\mathbf{X}_m = \mathbf{X}$ for use in future iterations and let $\mathbf{p}_0 = \mathbf{p}_n + \lambda \mathbf{X}$ be the new starting point for the next iteration.

The search directions for the first iteration are the parameter directions themselves.

Although the Powell algorithm has been found to be satisfactory for this application, there is no sense in which it is known to be the best method for fringe interpolation.

The coefficients of $\hat{B}(x_i)$ and $\hat{E}(x_i)$ are linear with respect to the irradiance distribution function $I(x)$. It should be mathematically much more efficient to find values for these coefficients with linear regression analysis. Only the coefficients of $\hat{P}(x_i)$ should be found with a nonlinear regression analysis algorithm such as that of Powell.

This work was sponsored by the U.S. Army Research Office.

References

1. H. E. Cline, A. S. Holik, and W. E. Lorensen, *Appl. Opt.* 21, 4481 (1982).
2. M. J. D. Powell, *Comput. J.* 7, 155 (1974).
3. L. H. Taylor and G. B. Brandt, *Exp. Mech.* 12, 543 (1972).
4. G. B. Brandt and L. H. Taylor, *Proc. Symposium on Engineering Applications of Holography Soc. Photo-Opt. Instrum. Eng.* 123 (1972).
5. J. E. Sollid, *Opt. Eng.* 14, 460 (1975).
6. R. Berggren, *Opt. Spectra* 12, 22 (1970).
7. E. R. Friere, O. E. Toler, and R. Race, *Opt. Eng.* 20, 253 (1981).
8. D. H. McLain, *Comput. J.* 17, 318 (1974).

Tomographic reconstruction of strongly refracting fields and its application to interferometric measurement of boundary layers

Soyoung Cha and C. M. Vest

An iterative algorithm for tomographic reconstruction of refractive-index fields from measured values of path integrals along rays which have been bent by refraction is presented. The behavior of the algorithm is studied by applying it to path length data obtained by computer simulation of experiments in which holographic or Mach-Zehnder interferograms of the field are recorded for several different viewing directions. A special form of the algorithm is also used to measure concentration profiles in the boundary layer formed at the cathode of an electrolytic cell containing ZnCl_2 . The Appendix contains a discussion of series expansion techniques for reconstructing object fields from measured values of line integrals through the field.

I. Introduction

The problem of reconstructing a refractive-index field from measured values of path integrals through it is of interest in optical interferometry^{1,2} and computer-assisted ultrasonic tomography.³⁻⁸ In this paper we address this problem in the context of measurement of fields in which refraction causes significant bending of the probing rays. Such strong refraction abrogates the direct applications of analytical⁹ and algebraic¹⁰ reconstruction techniques normally used for computer-assisted tomography because they are based on the assumption of straight probing rays. We present here an iterative scheme, outlined in a previous Letter,¹¹ for reconstructing strongly refracting refractive-index fields from data obtained by multidirectional holographic interferometry. The technique is based on ray optics and involves use of an imaging system during formation of the interferogram. Other authors have recently reported iterative schemes based on ray optics and algebraic reconstruction techniques for applications to computer-assisted ultrasonic tomography.⁴⁻⁸ The ultrasonic techniques reported to date differ substantially from the optical methods discussed herein because no

imaging is used. In fact, some of the most detailed work dealing with strong ultrasonic refraction⁶ involves the use of a transmitter-receiver pair, which scans laterally with the two elements fixed relative to each other as if mounted on a rigid bar. McKinnon and Bates¹² have shown that this data recording format can result in large areas within the object being inaccessible to tomography when refraction is significant.

In multidirectional interferometry, either a holographic² or Mach-Zehnder¹³ interferometer is used to record interferograms of some object field from a variety of viewing directions. Path length differences are measured by analyzing the fringe pattern formed when an optical wave that has passed through the test region interferes with some reference wave. In the case of double-exposure holographic interferometry, this reference wave is one that passes through the same test region in the absence of the object field. In the case of Mach-Zehnder interferometry, the reference wave is a plane wave, which spatially bypasses the object field before being recombined with the object wave. The following discussion applies to either case.

Figure 1 is a schematic diagram showing the formation of an interferogram. An imaging system, represented here by a single thin lens, is used to form a real image of a plane in the object defined by the coordinate r_j . The object refractive-index field is assumed to be within a circular region. Two rays intersect and interfere at a typical point P' in the image plane. One is the straight ray DEF through the undisturbed medium with refractive index n_0 . This ray is defined by its distance ρ from the optical axis. The other ray AB is curved due to refraction by the refractive-index field $n(r, \phi)$. This ray is located by projecting the emerging

The authors are with University of Michigan, Department of Mechanical Engineering & Applied Mechanics, Ann Arbor, Michigan 48109.

Received 24 December 1980.

0003-6935/81/162787-08\$00.50/0.

© 1981 Optical Society of America.

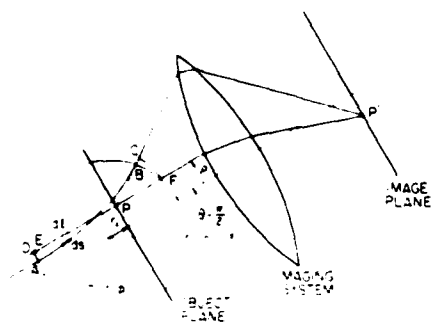


Fig. 1. Formation of an interferogram.

segment of ray \overline{AB} back along its tangent to the object plane, thereby defining the apparent object point P . If the light entering the object field is collimated and if the imaging system is ideal, no relative changes of optical path length between the two rays occur to the left of points A and D or to the right of points C and F . Point C is the intersection of the exiting refracted ray with a circular arc centered at P and passing through F . The optical path length difference of the two rays which interfere at point P' is therefore

$$\Delta\bar{\Phi}(\rho, \theta) = \int_1^n n(r, \phi) ds + n_0 (\overline{BC} - \overline{DE} - \overline{EF}) \quad (1)$$

The first term in Eq. (1) is the integral of the refractive index along the curved path \overline{AB} , which is a solution of the ray equation:

$$\frac{d}{ds} \left(n \frac{d\mathbf{r}}{ds} \right) = \nabla n \quad (2)$$

The optical path length difference is a nonlinear integral transform of $n(r, \phi)$, which is defined by Eqs. (1) and (2). We term this the path length transform and denote it by \bar{P} :

$$\Delta\bar{\Phi}(\rho, \theta) = \bar{P}[n(r, \phi); n_0] \quad (3)$$

For each viewing direction, defined by angle θ from some arbitrary reference direction, $\Delta\bar{\Phi}$ can be measured by determining the variation of fringe order number N_f with ρ :

$$\Delta\bar{\Phi}(\rho, \theta) = \lambda_0 N_f(\rho, \theta) \quad (4)$$

where λ_0 is the wavelength of light in the undisturbed medium with refractive index n_0 .

If the refractive-index variation is sufficiently small, the curved ray \overline{AB} in Fig. 1 will essentially coincide with the straight line \overline{EF} , and Eqs. (1) and (3) will reduce to

$$\Delta\bar{\Phi}(\rho, \theta) = \int_E^F [n(r, \phi) - n_0] dl \quad (5)$$

$$\bar{P}[n(r, \phi); n_0] = \bar{R}[n(r, \phi) - n_0] = \Delta\bar{\Phi}(\rho, \theta) \quad (6)$$

In Eqs. (5) and (6) the overbar denotes quantities defined for straight paths, dl is a differential distance along the straight line \overline{EF} , and \bar{P} is termed the line-integral transform which is mathematically equivalent to the 2-D Radon transform \bar{R} of $n(r, \phi) - n_0$.

In this paper a scheme for approximate inversion of the path length transform \bar{P} is presented. To date no analytical inversion of \bar{P} is known for the general asymmetric case, although such an inversion is known for the case of strongly refracting radially symmetric object fields $n(r)$.¹⁴ An extensive literature dealing with inversion of the line integral transform exists because it forms the basis of computer-assisted tomography.

In Sec. II we present an iterative scheme for reconstruction of a strongly refracting refractive-index field from measured values of its path length transform. In Sec. III we present measurements of mass concentration boundary layers which were obtained by applying the iterative reconstruction scheme to data obtained by holographic interferometry. The Appendix contains a discussion of the application of series expansion methods to inversion of the line integral transform; these methods are utilized as part of the iterative scheme.

II. Iterative Reconstruction of Strongly Refracting Fields

Appreciable errors may result if data representing the path length transform of a strongly refracting field are reconstructed by inversion codes designed for the ordinary case of tomography in the refractionless limit. We have used an iterative procedure for computational inversion of the path length transform. The method is based on successive estimation of the deviation function defined by

$$D(\rho, \theta) = \Delta\bar{\Phi}(\rho, \theta) - \Delta\bar{\Phi}(\rho, \theta) \quad (7)$$

It is assumed here that the domains of definition of $\Delta\bar{\Phi}$ and $\Delta\bar{\Phi}$ are the same. In some applications this is not the case, and a transform termed the T transform $T(\Delta\bar{\Phi})$ must be introduced to make the domains of definition identical.¹⁵

The iterative algorithm is as follows¹¹:

- (1) Make an initial estimate of the deviation function $D(\rho, \theta)$, where $i = 0$.
- (2) Calculate the corresponding estimate of the line integral transform, i.e., the refractionless path length transform

$$\Delta\bar{\Phi}(\rho, \theta) = \Delta\bar{\Phi}(\rho, \theta) - D(\rho, \theta) \quad (8)$$

- (3) Approximately reconstruct the field by computational inverse line-integral transformation:

$$n(r, \phi) - n_0 = \bar{P}^{-1} \Delta\bar{\Phi} \quad (9)$$

- (4) Using computational ray tracing, calculate the path length transform of the estimated field:

$$\Delta\bar{\Phi}(\rho, \theta) = \bar{P}[n(r, \phi); n_0] \quad (10)$$

- (5) Calculate a new estimate of the deviation function:

$$D(\rho, \theta) = \Delta\bar{\Phi} - \Delta\bar{\Phi} \quad (11)$$

- (6) Return to step (2) and continue the iterative procedure until the change of some measure of $D(\rho, \theta)$.

or of the difference between two successive reconstructed fields, is minimized or smaller than some predetermined value.

To implement this algorithm, we expressed the line-integral transform, which must be inverted in step (3), as a Fourier series within the circular domain $\rho/R \leq 1$:

$$\bar{\Delta}\Phi(\rho, \theta) = \sum_m \sum_n A_{mn} g_{mn}(\rho) \exp(im\theta), \quad (12)$$

where $g_{mn}(\rho)$ is the product of an orthogonal polynomial and an envelope function whose specific forms are discussed in the Appendix. A finite number of coefficients A_{mn} are calculated by fitting them to the known discrete values of the line-integral transform $\Delta\Phi(\rho_i, \theta_i)$. In theory this could be done by the usual methods of Fourier analysis. In practice, redundant data were recorded in an attempt to suppress amplification of input errors, that is, a number of coefficients A_{mn} less than the number of given values of $\Delta\Phi(\rho_i, \theta_i)$ were calculated by solving the overdetermined system of algebraic equations

$$\bar{\Delta}\Phi(\rho_i, \theta_i) = \sum_m \sum_n A_{mn} g_{mn}(\rho_i) \exp(im\theta_i) \quad (13)$$

in the least squares sense using the subroutine *DLLSQ*¹⁶ based on an algorithm due to Golub.¹⁷ Once the coefficients A_{mn} have been calculated, the reconstructed distribution of change of refractive index, $f(r, \phi) = n(r, \phi) - n_0$, can be represented by a Fourier series within the circular domain $r/R \leq 1$:

$$f(r, \phi) = \sum_m \sum_n A_{mn} f_{mn}(r) \exp(im\phi) \quad (14)$$

Appropriate functions $g_{mn}(\rho)$ and $f_{mn}(r)$ which are line-integral transform pairs are discussed in the Appendix and in more detail in the thesis of Cha.¹⁵

We chose the approach of series expansion of the field and its transform because it is convenient for accurate and efficient computational ray tracing and because the fields to which we intend to apply the code have relatively smooth structures. The series expansion approach used in our investigations yielded a fairly efficient reconstruction code, and the matrix of the equations for A_{mn} is relatively sparse. The only nonzero coefficients A_{mn} are those for which

$$\begin{aligned} m &= 0, \pm 1, \pm 2, \pm 3, \dots \\ n &= |m| + 2l, \\ l &= 0, 1, 2, 3, \dots \end{aligned} \quad (15)$$

In step (4) of the algorithm, the path length transform of an estimated refractive-index field must be computed. Because the refractive-index distribution is expressed in analytical form, namely, by a series as in Eq. (14) rather than by values at discrete points, we found it convenient to base the ray tracing procedure on the use of Hamilton's equations¹⁸ rather than on Snell's law or direct integration of the ray equation. Indeed a modified form of Hamilton's equations can be obtained by decomposing the ray equation [Eq. (2)] into an equivalent set of first-order equations. There are

advantages in terms of accuracy and computation time to such decomposition.¹⁹ In Cartesian coordinates, the equations are

$$\frac{dy}{dx} = \tan \gamma, \quad (16a)$$

$$\frac{d\gamma}{dx} = \frac{\frac{\partial n}{\partial y} - \frac{\partial n}{\partial x} \tan \gamma}{n}, \quad (16b)$$

$$\frac{d(\Delta E)}{dx} = \frac{n}{\cos \gamma}, \quad (16c)$$

where $\Delta\gamma$ is the angle between the tangent to the ray and the x axis. ΔE is the optical path length of the ray, which, when evaluated as the ray exits the circular region $r/R \leq 1$, is the value of the integral appearing in the path length transform, Eq. (1). The corresponding system in polar coordinates is

$$\frac{d\phi}{dr} = \frac{1}{r} \tan \phi, \quad (17a)$$

$$\frac{d\chi}{dr} = \frac{1}{rn} \left[-\frac{\partial n}{\partial r} \left(r \frac{\partial n}{\partial r} + n \right) \tan \chi \right], \quad (17b)$$

$$\frac{d(\Delta E)}{dr} = \frac{n}{\cos \chi}, \quad (17c)$$

where ϕ is the polar angle from the x axis to the radial position vector of a point on the ray, and χ is the angle between the tangent to the ray at that point and the radial position vector. After testing several numerical integration schemes with regard to computational efficiency for this application, we chose to use the subroutine package *DRIVE*²⁰ to integrate Eqs. (16) or (17). A variable-order variable-step-size differential equation solver of the Adams type based on Gear's subroutine *DIFSUB*²¹ was used. The path length transforms required in step (4) were computed in this manner for sets of equally spaced parallel rays entering the region $r/R \leq 1$. Cubic spline interpolation was used to estimate $\Delta\Phi(\rho, \theta)$ corresponding to other ray paths through the field.

The path length transform depends in part on the object plane selected by the observer when the image of the interference pattern is formed. The importance of the selection of this plane is evidenced by the fact that if the object field is radially symmetric, the deviation function can be experimentally reduced nearly to zero by focusing on the center plane of the object.²² A similar effect occurs in boundary layer-type fields around objects of length L if one focuses a distance $L/3$ from the exit plane.²² If the object field is asymmetric, the observer should select an object plane in which no apparent ray crossing occurs and in which the fringe spacing across the interferogram is fairly uniform.

During operation of the algorithm, crossing of computed rays through the estimated field can occur. The computer code should include logic to recognize such occurrences and discard the corresponding computed values of $\Delta\Phi$.

The behavior of the algorithm was studied by applying it to data generated by numerical simulation of interferometry experiments. Discrete values of the

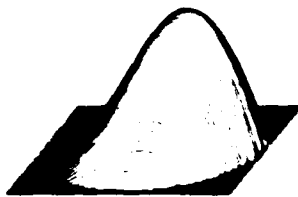


Fig. 3. Reconstruction of the axisymmetric refractive-index distribution described by Eq. (19): (a) field and its reconstruction; (b) reduction of error by iterative reconstruction.

path length transform were generated by computational ray tracing through test object fields expressed in analytical form. The transform was computed for several different object planes, from which one was selected using the criteria noted above. After each iteration the current estimate of the object field was recorded, and the maximum error and average error over the field were computed as percentages of the maximum refractive-index change. In all cases, $n_0 = 1$.

Figure 2(a) is a plot of the absolute value of an asymmetric object field expressed as

$$n - n_0 = -0.06[1 - (r/R)^2][(x/R) + 1.5]^2. \quad (18)$$

The simulated data consisted of thirty-one equally spaced values of $\Delta\Phi$ for each of eight viewing directions spaced at equal angular intervals over a 180° range of viewing directions. This field refracts quite strongly, bending some rays by as much as 27° . The reduction of maximum and average errors by the iterative procedure is shown in Fig. 2(b). In this figure, and in those that follow, iteration 1 refers to reconstruction by assuming that $\Delta\Phi = \Delta\phi$, i.e., refraction is neglected.

Figure 3 shows the results of reconstructing a radially symmetric distribution which has a single maximum and decays gently to n_0 at $r = R$:

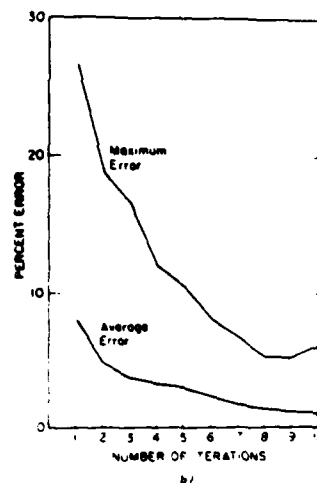
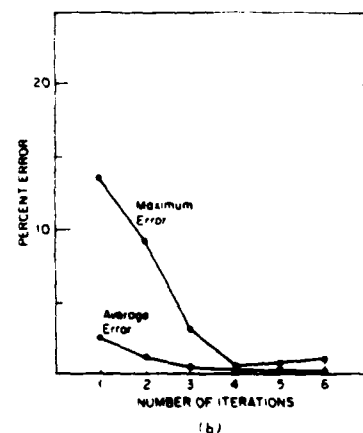
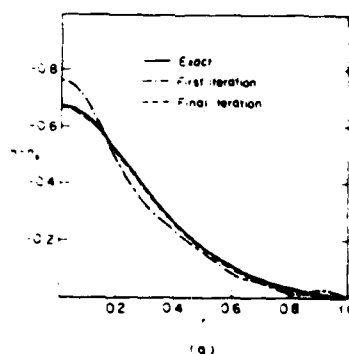


Fig. 2. Reconstruction of an asymmetric object field: (a) plot of the absolute value of the refractive-index distribution described by Eq. (18); (b) reduction of error by iterative reconstruction of this field.



$$n(r) - n_0 = 1 - 0.9 \exp[-4(r/R)^2]^{1/2}. \quad (19)$$

Figure 4 shows the results of reconstructing a radially symmetric field which has two local maxima and which decays rather abruptly to n_0 at the boundary

$$n(r) - n_0 = -0.05[1 - (r/R)^2] + 0.025[\cos(3\pi r/R) + 1]. \quad (20)$$

Although our study of performance of the algorithm was limited in scope, some conclusions can be drawn. Care must be exercised in selecting parameters such as the position of the object plane (r_f in Fig. 1), the number of terms in the series used to represent the object field and its transform, and the number of rays traced to calculate estimates of the path length transform. The principal factor in determining computation time is the number of terms in the series, because the series must be evaluated many times during ray tracing. One way of reducing the number of terms is to use an envelope function whose form is generally similar to the expected form of the field being measured. This concept is described in the Appendix, and its application is illustrated in the next section. Although we have demonstrated successful reconstruction of fields with multiple maxima and quite steep gradients, there are surely limitations to the complexity of fields which can be accurately reconstructed using limited data and com-

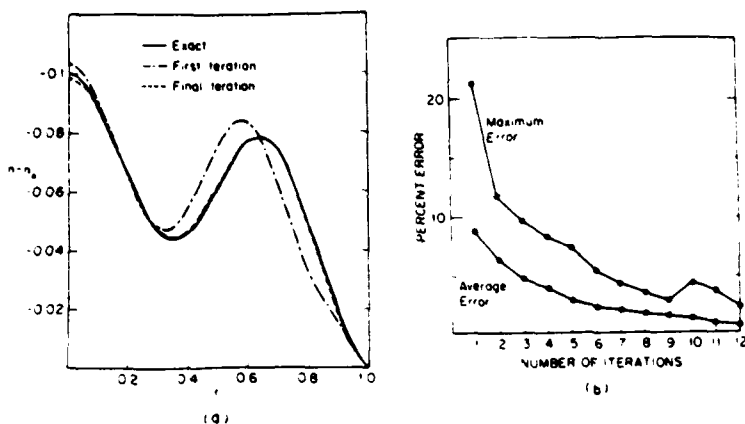


Fig. 4. Construction of the axisymmetric refractive-index distribution described by Eq. (20): (a) field and its reconstruction; (b) reduction of error by iterative reconstruction.

puting power. Such limitations are probably set by excessive ray crossing and oscillation of estimated ray paths near closely spaced peaks and valleys in the refractive-index distribution.

III. Application to Measurement of Mass Transfer Boundary Layers

A specialized computer code based on the algorithm presented in Sec. II was written for use in measuring strongly refracting boundary layers. It was applied to interferometric measurements of the concentration boundary layer on the cathode of an electrolytic cell filled with ZnCl_2 . Figure 5 is a schematic diagram of a test cell in which a boundary layer is formed on the surface of some opaque object. The refractive index within the boundary layer varies rapidly and monotonically in the direction normal to the object surface but does not vary appreciably parallel to the surface. The refractive index of undisturbed fluid in the cell is n_0 ; the refractive index of air outside the cell is n_a ; and the refractive index of the window is n_w .

We assume that the interferogram is formed by two-exposure holography. During the first exposure the fluid has a uniform refractive index n_0 , and during the second exposure the boundary layer, whose refractive index $n(x)$ is to be determined, is present adjacent to the opaque surface. The thickness of the boundary layer is δ_b . Optical rays which are near the outer edge of the boundary layer, $x \approx \delta_b$, are nearly undeflected, but those which enter adjacent to the surface, $x = 0$, are strongly refracted. Hence, in the interferogram, the object surface will appear to be displaced as shown in Fig. 5. The amount of displacement depends on the choice of object plane. If the opaque surface is physically present during both holographic exposures the observer must focus on the one object plane in which both images of the surface appear to coincide; however, apparent ray crossing or diffraction patterns may make the interferogram difficult to read near the object surface. An alternative is to remove physically the opaque surface during the first holographic exposure. In this case, which is optically equivalent to Mach-Zehnder

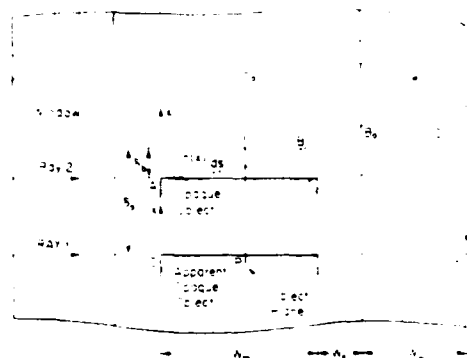


Fig. 5. Refraction of an optical ray by a boundary layer and test section window. Apparent displacement of the object surface and an appropriate distortion of the boundary layer result.

interferometry, the observer is free to choose an arbitrary object plane in which no apparent ray crossing occurs and in which the fringes are more numerous and more uniformly distributed. We assume this latter case in the following discussion since it is general.

The path length transform is

$$\begin{aligned} \tilde{P}[n(x); n_0] &= \Delta \tilde{\Phi}(x') \\ &= \int_0^{\delta_b} n(x) dx + n_0 \overline{BB_0} - n_0 \overline{AA_0} - n_0 \overline{CC_0} \\ &\quad + n_a (\overline{BB_0} - \overline{AA_0}) - n_a \overline{CC_0} \end{aligned} \quad (21)$$

$$\tilde{P}[n(x); n_0] = \Delta \tilde{\Phi}(x') = n_M [n(x) - n_0] \quad (22)$$

where x' is the coordinate measured from the apparent location of the opaque surface. \tilde{P} is defined over a region of width δ_a , the apparent boundary layer thickness, but \tilde{P} is defined over a region of width δ_b . To apply the algorithm, the coordinates must therefore be stretched by applying what we term the T transform:

$$T[\Delta \tilde{\Phi}(x)] = p \Delta \tilde{\Phi}(x/p) \quad (23)$$

where $p \equiv \delta_b/\delta_a$. The line-integral transform was expanded in a polynomial series multiplied by an envelope function:

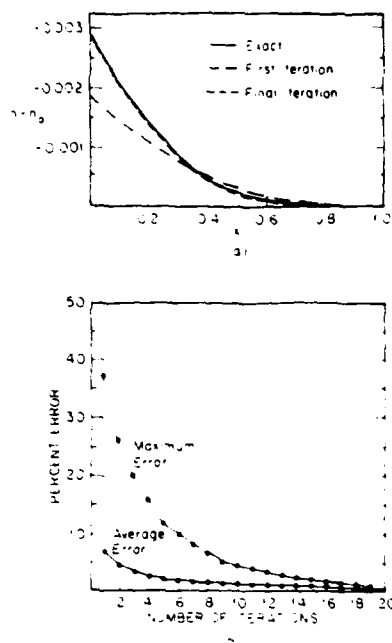


Fig. 6. Reconstruction of a boundary layer with refractive index $n(x) = n_0 = -0.003 \operatorname{erfc}(2.5x)$ imaged so that $p = 2.05$: (a) distribution and its reconstruction; (b) reduction of errors by iterative reconstruction.

$$\Delta \bar{p}(x) = e(x) \sum_{j=1}^N A_j x^j \quad (24)$$

Prior to experimental work, several computer simulations were carried out. One example is the test model:

$$\begin{aligned} n(x) = n_0 &= -0.003 \operatorname{erfc}(2.5x) & n_0 &= 1.3311; \\ n_1 &= 1.5231 & n_2 &= 1.0002674; \\ n_3 &= 12.7 \text{ mm} & n_4 &= 0; \\ n_5 &= 20.00 \text{ mm} & \delta_s &= 1.0 \text{ mm}. \end{aligned}$$

Here erfc denotes the complimentary error function. Figure 6(a) shows the iterative improvement of the reconstruction when the plane is chosen so that $p = 2.05$. Similar results are shown in Fig. 7 for the case of $p = 1$, i.e., when the two images of the surface coincide. In both cases, ten simulated fringe readings were used, the approximating series had five terms, and a linear envelope function $e(x) = 1 - x/\delta_s$ was used. The simulations indicate good accuracy and convergence.

The test cell used in the mass transfer experiments was a Plexiglas tank with flat quartz windows. The dimensions of the cell were selected on the basis of the results of simulated experiments. During the experiments, natural convection was induced by differences in concentration of ZnCl_2 across the 3-mm wide gap between the cathode and a flat porous graphite diaphragm. The cathode was an accurately machined graphite bar, and the anode was a zinc rod inserted into the ZnCl_2 solution on the other side of the diaphragm. Some physical properties and dimensions were

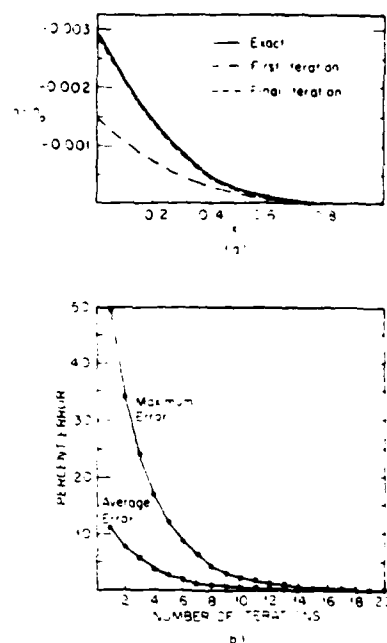


Fig. 7. Reconstruction of the same boundary layer as in Fig. 6 imaged so that $p = 1.0$: (a) distribution and its reconstruction; (b) reduction of errors by iterative reconstruction.

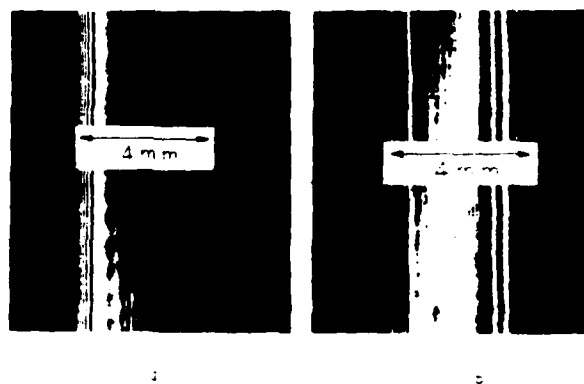


Fig. 8. Interferogram of a portion of the cathodic boundary layer: (a) current density 5 mA/cm; (b) current density 15 mA/cm.

$$\begin{aligned} n_1 &= 1.0002674 & n_2 &= 1.3695 & n_3 &= 1.4571; \\ n_4 &= 5 \text{ mm} & n_5 &= 3 \text{ mm} & n_6 &= 6.35 \text{ mm} \end{aligned}$$

Holograms were recorded on Agfa Gevaert 10E75 plates using a 50-mW He-Ne laser. The first exposure was recorded with a homogeneous solution with concentration $C_0 = 1.5$ mole/liter of ZnCl_2 in water at 20°C . An electrical potential difference was then applied across the electrodes, and the second exposure was recorded after the cell had stabilized for 5 min. The interferograms were recorded by photographing the holographic virtual image through an afocal telescope

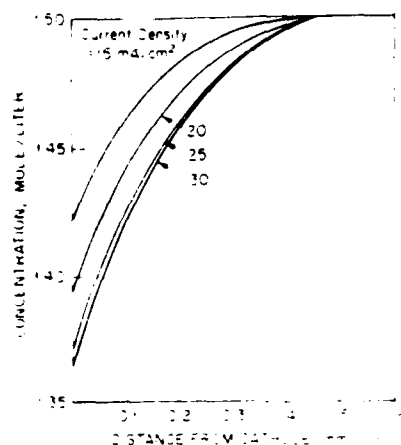


Fig. 9. Reconstructed boundary layer concentration profiles.

formed by two 628-mm lenses. The interferograms were then enlarged by a factor of ~ 14 . Fringe positions in the enlarged photographs were measured with a micrometer-driven translating microscope. Interferograms recorded with cathodic current densities of 3 and 15 mA/cm² are shown in Fig. 8.

Using the computer code described above, the refractive-index distribution in the boundary layer was measured for several different current densities. Concentration distributions were then inferred by using the relation

$$C - C^* = 52.63(n - n_{cl}) \quad (25)$$

which was determined by refractometry. Typical boundary layer profiles determined in this manner are shown in Fig. 9. We were able to measure boundary layer profiles for current densities up to ~ 30 mA/cm². This effective upper limit was set by the loss of ability to resolve individual fringes in the background noise using the available optical system. Other physical factors such as generation of additional ionic species at high current densities also limit the accuracy of concentration measurements.

This work was supported by the National Science Foundation (grant ENG76-21421) and in part by the U.S. Army Research Office. We also wish to acknowledge the support of the experimental work by Energy Development Associates, Inc.

Appendix

We utilized a series expansion method to invert the line-integral transform, i.e., the 2-D Radon transform of fields defined within a circular domain $|r| < R$. For simplicity, let $f(r, \phi)$ denote the field to be reconstructed and let $g(\rho, \theta)$ denote its line-integral transform. The objective is to expand $g(\rho, \theta)$ in a Fourier series and then invert that series term by term to obtain $f(r, \phi)$. In practice $g(\rho, \theta)$ is obtained by physical measurements, in this case by interferometry. To speed convergence of the series and consequently decrease computation

time we found it convenient to introduce the concept of an envelope function, $e(r/R)$, which is a function having roughly the same radial shape as $f(r, \phi)$; similarly $e(\rho/R)$ has roughly the same radial shape as $g(\rho, \theta)$. It is not difficult to choose an appropriate $e(\rho/R)$ by examining the data. We now show how an appropriate series can be chosen and inverted once $e(\rho/R)$ has been selected.

Let D be the space of all functions in 2-D space which have support, are continuous, and are bounded in $|r| < R$. Furthermore, let $D_{(r, R)}$ be the space spanned by functions in D multiplied by $e(r/R)$, which is assumed to be an even function which has support, is continuous, and Lebesgue integrable in $|r| < R$.

Using results set forth by Ludwig²³ and the envelope function concept, it can be shown that the necessary and sufficient conditions for $g(\rho, \theta)$ to be the 2-D Radon transform of $f(r, \phi)$ in $D_{(r, R)}$ are that

- (1) $g(-\rho, \theta)$ is a function in $D_{(\rho, R)}[1 - (\rho/R)^2]^{-1/2}$
- (2) $g(\rho, \theta + \pi) = g(\rho, \theta)$;
- (3) $\int_{-\pi}^{\pi} \int_0^R g(\rho, \theta) \rho^k \exp(\pm i m \theta) d\rho d\theta = 0$ if $m > k$ for arbitrary $k \geq 0$.

The line-integral transform of any function in $D_{(r, R)}$ can be expanded in a series of circular harmonics and orthogonal polynomials. If we choose orthogonal polynomials $q_n(\rho/R)$ with weight function $e(\rho/R)[1 - (\rho/R)^2]^{-1/2}$ and utilize conditions (1)-(3), it can be shown that the appropriate series is of the form

$$g(\rho, \theta) = \sum_{n=0}^{\infty} \left(\frac{\rho}{R} \right) \left[1 - \left(\frac{\rho}{R} \right)^2 \right]^{-1/2} \sum_{m=-\infty}^{\infty} \sum_{k=-\infty}^{\infty} A_{k+m,n} q_n \left(\frac{\rho}{R} \right) \exp(\pm i m \theta) \quad (26)$$

The notation $n = m, 2$ indicates that n increases in increments of 2 from a lower limit m , i.e., only about a third of the coefficients in the series are nonzero.

The inverse transform can be found on a term-by-term basis using the following relation among the inverse Radon transform R^{-1} , the 1-D Fourier transform F , and the Hankel transform of order m , H_m (Ref. 24):

$$R^{-1} [g(\rho, \theta) \exp(\pm i m \theta)] = f_m(r) \exp(\pm i m \theta), \quad (27)$$

where $f_m(r) = i^{-m} H_m[F[g_m(\rho)]]$. Here the definitions of the transforms are

$$H_m[f(x)] = 2\pi \int_0^\infty f(x) J_m(2\pi x t) x dx, \quad (28)$$

$$F[f(x)] = \int_{-\infty}^\infty f(x) \exp(-i 2\pi x t) dx, \quad (29)$$

where $J_n(x)$ is the Bessel function of the first kind of order n . The following three expansions and their inverses are typical results of this approach:

- (1) Let the envelope function $e(\rho/R) = 1$ on the disk $\rho/R \leq 1$, then the expansion of the transform $g(\rho, \theta)$ is

$$g(\rho, \theta) = \sum_{n=0}^{\infty} \sum_{m=-\infty}^{\infty} A_{k+m,n} P_n \left(\frac{\rho}{R} \right) \exp(\pm i m \theta), \quad (30)$$

where $P_n(\rho)$ is the Legendre polynomial of degree n . The inverse transform is

$$f(r, \phi) = \frac{1}{\pi R [1 - (r/R)^2]^{1/2}} \sum_{m=0}^{\infty} \sum_{n=m,2}^{\infty} A_{\pm m, n} \cdot \frac{(-1)^{(m-n)/2} (1 - \frac{r^2}{R^2})^{\frac{n-m}{2}}}{\Gamma_2(n-m)} \left(\frac{r}{R}\right)^m P_{\frac{n-m}{2}}^{\frac{n-m}{2}} \times \left[1 - 2\left(\frac{r}{R}\right)^2\right] \exp(\pm im\phi). \quad (A6)$$

This expansion was first presented by Cha.¹⁵

(1) Let the envelope function $e(\rho/R) = [1 - (\rho/R)^2]^{1/2}$ on the disk $\rho/R \leq 1$; then the expansion of the transform $g(\rho, \theta)$ is

$$g(\rho, \theta) = \left[1 - \left(\frac{\rho}{R}\right)^2\right]^{1/2} \sum_{m=0}^{\infty} \sum_{n=m,2}^{\infty} A_{\pm m, n} U_n\left(\frac{\rho}{R}\right) \exp(\pm im\theta), \quad (A7)$$

where $U_n(\rho)$ is the Chebyshev polynomial of the second kind of degree n . The inverse transform is

$$f(r, \phi) = \frac{1}{2R} \sum_{m=0}^{\infty} \sum_{n=m,2}^{\infty} A_{\pm m, n} U_n\left(\frac{r}{R}\right) P_{\frac{n-m}{2}}^{\frac{n-m}{2}} \times \left[2\left(\frac{r}{R}\right)^2 - 1\right] \exp(\pm im\phi), \quad (A8)$$

where $P_n^{(\alpha, \beta)}(r)$ is the Jacobi polynomial of degree n . This expansion and inverse were derived by Cormack.²⁵

(3) Let the envelope function $e(\rho) = \exp(-\alpha^2 \rho^2)$ and let f and g be defined on the entire plane; then the expansion of the transform $g(\rho, \theta)$ is

$$g(\rho, \theta) = \exp(-\alpha^2 \rho^2) \sum_{m=0}^{\infty} \sum_{n=m,2}^{\infty} A_{\pm m, n} H_n(\alpha \rho) \exp(\pm im\theta), \quad (A9)$$

where $H_n(\alpha \rho)$ is the Hermite polynomial of degree n . Its inverse transform is

$$f(r, \phi) = \frac{\alpha}{\sqrt{\pi}} \exp(-\alpha^2 r^2) \sum_{m=0}^{\infty} \sum_{n=m,2}^{\infty} A_{\pm m, n} (-1)^{(n-m)/2} (1 - \frac{r^2}{2})^{\frac{n-m}{2}} (\alpha r)^m \times L_{\frac{n-m}{2}}^{\frac{n-m}{2}}(\alpha^2 r^2) \exp(\pm im\phi), \quad (A10)$$

where

$$(a)_0 = 1,$$

$$(a)_n = a(a+1)(a+2)\dots(a+n-2)(a+n-1),$$

and $L_n^{\alpha}(r)$ is the associated Laguerre polynomial of degree n . This expansion and inverse were derived by Maldonado and Olsen.²⁶

The computational inversions of line integral transforms performed while computing the reconstructions reported in Sec. II were based on a modification of Eqs. (A5) and (A6). This modification resulted from introducing the additional constraint that $g(R, \theta) = 0$, i.e., that the transform vanishes at $\rho = R$. This results in the following expansion of the transform $g(\rho, \theta)$:

$$g(\rho, \theta) = \sum_{m=0}^{\infty} \sum_{n=m+2,4,6,\dots}^{\infty} A_{\pm m, n} \left[P_n\left(\frac{\rho}{R}\right) - P_n\left(\frac{R}{R}\right) \right] \exp(\pm im\theta). \quad (A11)$$

The inverse transform is

$$f(r, \phi) = \frac{1}{\pi R} [1 - (r/R)^2]^{1/2} \sum_{m=0}^{\infty} \sum_{n=m+2,4,6,\dots}^{\infty} A_{\pm m, n} \exp(\pm im\phi) \left(\frac{r}{R}\right)^n \times \left[\frac{(-1)^{(m-n)/2} (m+1) \Gamma_2(\frac{n-m}{2})}{(1/2) \Gamma_2(\frac{n-m}{2})} \left(\frac{m-n}{2}\right)_* \left(\frac{m-n+1}{2}\right)_* \right]$$

$$\cdot \left(\frac{r}{R}\right)^{2k} \left[1 - \left(\frac{r}{R}\right)^2 \right]^{\frac{(m-n-1-k)}{2}} - \sum_{k=0}^{\frac{n-m-1}{2}} \left(\frac{r}{R}\right)^{2k} \right]. \quad (A12)$$

Equation (A12) has been presented in a form, which, although cumbersome, is suitable for computation and which explicitly indicates that this approach results in the envelope function $[1 - (r/R)^2]^{1/2}$.

References

1. D. W. Sweeney and C. M. Vest, *Appl. Opt.*, **12**, 2649 (1973).
2. C. M. Vest, *Holographic Interferometry* (Wiley, New York, 1979), Chap. 6.
3. B. P. Hildebrand and D. E. Hufford, in *Acoustical Holography*, Vol. 7, L. W. Kessler, Ed. (Plenum, New York, 1976), pp. 245-262.
4. A. C. Kak, *Proc. IEEE*, **67**, 1245 (1979).
5. J. F. Greenleaf, S. A. Johnson, W. F. Samayo, and F. A. Duck, in *Acoustical Holography*, Vol. 6, N. Booth, Ed. (Plenum, New York, 1975), pp. 71-90.
6. J. A. Greenleaf and S. A. Johnson, *Ultrasound Med. Biol.*, **3**, 127 (1978).
7. G. H. Glover and J. C. Sharp, *IEEE Trans. Sonics Ultrason.*, **SU-24**, 229 (1977).
8. H. Schomberg, *J. Phys. D*, **11**, L181 (1978).
9. K. T. Smith, D. C. Solomon, and S. L. Wagner, *Bull. Am. Math. Soc.*, **83**, 1227 (1977).
10. R. Gordon and G. T. Herman, *Int. Rev. Cytol.*, **38**, 111 (1974).
11. S. Cha and C. M. Vest, *Opt. Lett.*, **4**, 311 (1979).
12. G. C. McKinnon and R. H. T. Bates, *Ultrason. Imaging*, **2**, 45 (1980).
13. H. Krauss, "Ein Auswertverfahren für allgemeine dreidimensionale Dichtefelder mit Hilfe der Interferenzmethode," Doctoral Dissertation, U. Stuttgart (1977).
14. C. M. Vest, *Appl. Opt.*, **14**, 1601 (1975).
15. S. Cha, "Reconstruction of Strongly Retracting Asymmetric Fields from Interferometric Measurements," Doctoral Dissertation, U. Michigan, Ann Arbor (1980).
16. *IBM Application Program - System 160 Scientific Subroutine Package (360 A-C Mod X), Version III, Programming Manual* (IBM, White Plains, N.Y., 1970).
17. G. Golub, *Numer. Math.*, **7**, 206 (1965).
18. J. L. Synge, *Hamilton's Method in Geometrical Optics*, Institute for Fluid Dynamics and Applied Mathematics, U. Maryland, 1951, Lecture Series 9.
19. B. Carnahan, H. A. Luther, and J. O. Wilkes, *Applied Numerical Methods* (Wiley, New York, 1969).
20. A. C. Hindmarsh, *Gear - Ordinary Differential Equation Solver*, Report UCID-30001, Rev. 3, Lawrence Livermore Laboratory (1974).
21. C. W. Gear, *Numerical Initial Value Problems in Ordinary Differential Equations* (Prentice-Hall, Englewood Cliffs, N.J., 1971).
22. W. L. Howes and D. L. Buchele, *J. Opt. Soc. Am.*, **56**, 127 (1966).
23. D. Ludwig, *Commun. Pure Appl. Math.*, **19**, 49 (1965).
24. M. Ein-Gal, Tech. Report 6551-1, Information Systems Laboratory, Stanford U. (1974).
25. A. M. Cormack, *J. Appl. Phys.*, **35**, 2908 (1964).
26. C. D. Maldonado and H. N. Olsen, *J. Opt. Soc. Am.*, **56**, 127 (1966).

5